Structure-based development of new RAS-effector inhibitors from a combination of active and inactive RAS-binding compounds

Abimael Cruz-Migoni[a,b,1], Peter Canning[a,1,2], Camilo E. Quevedo[a,1], Carole J. R. Bataille[c], Nicolas Bery[a], Ami Miller[a], Angela J. Russell[c], Simon E. V. Phillips[b,d], Stephen B. Carr[b,d], and Terence H. Rabbitts[a,3]

[a]Weatherall Institute of Molecular Medicine, MRC Molecular Haematology Unit, John Radcliffe Hospital, University of Oxford, OX3 9DS Oxford, United Kingdom; [b]Research Complex at Harwell, Rutherford Appleton Laboratory, OX11 0FA Didcot, United Kingdom; [c]Chemistry Research Laboratory, University of Oxford, OX1 3TA Oxford, United Kingdom; and [d]Department of Biochemistry, University of Oxford, OX1 3QU Oxford, United Kingdom

Edited by James A. Wells, University of California, San Francisco, CA, and approved December 17, 2018 (received for review July 6, 2018)

The *RAS* gene family is frequently mutated in human cancers, and the quest for compounds that bind to mutant RAS remains a major goal, as it also does for inhibitors of protein–protein interactions. We have refined crystallization conditions for $KRAS_{169}^{Q61H}$-yielding crystals suitable for soaking with compounds and exploited this to assess new RAS-binding compounds selected by screening a protein–protein interaction-focused compound library using surface plasmon resonance. Two compounds, referred to as PPIN-1 and PPIN-2, with related structures from 30 initial RAS binders showed binding to a pocket where compounds had been previously developed, including RAS effector protein–protein interaction inhibitors selected using an intracellular antibody fragment (called Abd compounds). Unlike the Abd series of RAS binders, PPIN-1 and PPIN-2 compounds were not competed by the inhibitory anti-RAS intracellular antibody fragment and did not show any RAS-effector inhibition properties. By fusing the common, anchoring part from the two new compounds with the inhibitory substituents of the Abd series, we have created a set of compounds that inhibit RAS-effector interactions with increased potency. These fused compounds add to the growing catalog of RAS protein–protein inhibitors and show that building a chemical series by crossing over two chemical series is a strategy to create RAS-binding small molecules.

cancer | RAS | drugs | antibody | intracellular antibody

The oncogenic family of *RAS* genes is of significant interest in the fight against cancer because of the frequency of activating mutations (1). Their presence in almost all major cancers makes them a highly valued therapeutic target, in particular the KRAS gene, since it has been identified as one of the most frequently mutated oncogenes (2, 3). RAS proteins are linked to the plasma membrane by COOH-terminal prenylation mediated by farnesyl transferases (4). All family members function by signal transduction to the nucleus of cells via interaction with effectors (such as RAF, RALGDS, and PI3K) that catalyze phosphorylation of downstream proteins (5). When KRAS is bound to GDP, the protein is in the inactive state and becomes activated by nucleotide exchange from GDP to GTP. Normally, the activation/deactivation cycle is catalyzed by guanine nucleotide exchange factors and GTPase-activating proteins (GAPs) (6, 7). Mutant RAS proteins remain in the active state and hydrolyze GTP at a much slower rate than wild-type (WT) RAS (8). Mutations reduce GAP activity leading to constitutive activation of RAS effector pathways (2), constantly generating a signaling cascade that activates cell functions such as division, survival, and invasion (9).

Despite its great potential as a cancer target, KRAS has proved to be very difficult to inhibit in a therapeutic setting. KRAS signaling works via protein–protein interactions (PPI) that can be very difficult to disrupt (10). In addition, the nucleotides that regulate KRAS function (GTP and GDP) bind to the protein with picomolar affinity, making them problematic to displace (11). Attempts at targeting RAS function using farnesyl transferase inhibitors also proved to be ineffective, failing to demonstrate antitumor activity in KRAS-driven cancers (12). As an alternative to compounds, various macromolecules [called macrodrugs (13)] have been developed that can bind to RAS and prevent PPI with the RAS effectors, such as has been shown with intracellular antibody fragments (14, 15). The possible clinical use of these macrodrugs has not been implemented thus far due to difficulties in their delivery into cells, although methods are becoming available that may solve this problem (16).

Although there are a large number of mutant RAS protein isoforms, their structural conformation is highly conserved (17) because of the invariant N-terminal domain up to amino acid 166. The interest in inhibition of RAS proteins by small molecules has increased again recently (18), and several compounds have been described that bind to RAS (19–27). Recently, we have defined a chemical series based on an intracellular antibody-binding domain (28) that interact with a hydrophobic pocket (designated pocket I, *SI Appendix*, Fig. S1*A*), previously identified in silico (29) and confirmed as the binding site for 4,6-dichloro-2-methyl-3-aminoethyl-indole (DCAI) near the switch I region of KRAS (23).

Significance

The RAS family of oncogenic proteins is important as therapy targets because of the frequency of activating mutations in almost all major cancers. An important approach is development of small molecules with drug-like properties that can inhibit RAS-effector protein interactions inside cells. We present a strategy for identification of such compounds, and their development as RAS-effector interaction inhibitors, utilizing a structure-based design approach and cell-based assays. By combining moieties from two distinct sets of RAS-binding molecules, we generated cross-over compounds that showed improved efficacy in vitro and in cell-based assays.

Author contributions: C.E.Q. and T.H.R. designed research; A.C.-M., P.C., C.J.R.B., N.B., and A.M. performed research; A.C.-M., P.C., C.E.Q., C.J.R.B., N.B., A.M., A.J.R., S.E.V.P., S.B.C., and T.H.R. analyzed data; and A.C.-M., P.C., C.E.Q., C.J.R.B., N.B., A.M., S.E.V.P., S.B.C., and T.H.R. wrote the paper.

The authors declare no conflict of interest.

This article is a PNAS Direct Submission.

Data deposition: The atomic coordinates have been deposited in the Protein Data Bank, www.wwpdb.org (PDB ID codes 6GOD, 6GOE, 6GOF, 6GOG, 6GOM, 6GQT, 6GQW, 6GQX, and 6GQY).

[1]A.C.-M., P.C., and C.E.Q. contributed equally to this work.

[2]Present address: Assay Development, LifeArc, Open Innovation Campus, SG1 2FX Stevenage, United Kingdom.

[3]To whom correspondence should be addressed. Email: terence.rabbitts@imm.ox.ac.uk.

This article contains supporting information online at www.pnas.org/lookup/suppl/doi:10.1073/pnas.1811360116/-/DCSupplemental.

A critical step in drug development programs for progressing small molecules is the use of X-ray crystallography with compounds after crystal soaking or cocrystallization to identify where such molecules bind to the target protein. We have optimized $KRAS_{169}^{Q61H}$ crystallization and applied crystal soaking to assess a set of RAS-binding compounds selected from an initial diverse PPI-net 1 compound library (kindly provided by Andrew Wilson, University of Leeds, Leeds, UK), of which two bind in pocket I. However, unlike our previous Abd compounds, their binding was not impaired by binding of an inhibitory anti-RAS intracellular antibody fragment nor did they interfere with RAS-effector interactions. Comparison of the structures of these two PPI-net RAS-binding compounds and the lead compound Abd-7 allowed us to synthesize chimeric cross-over compounds that bind to RAS with improved potency and inhibit RAS-effector interactions whereas the PPI-net did not.

Results

Crystallography Conditions for $KRAS_{169}^{Q61H}$ GppNHp, Suitable for Crystal Soaking. Initially, we wanted to establish crystallization conditions to obtain a crystal form that would allow free movement of RAS-binding compounds through the lattice for crystal soaking. We reproduced the $KRAS_{169}^{Q61H}$ crystal structure found in the database (PDB ID code 3GFT) but with optimized crystallization conditions, using sparse matrix crystallization screening with a protein spanning residues 1–169. This produced diffraction quality crystals that showed similar packing to PBD ID code 3GFT with six chains in the asymmetric unit (Fig. 1*A* and *SI Appendix*, Table S1). All six crystallographically independent chains (identified as chains A–F) have the same fold. Noncrystallographic symmetry averaging of the electron density maps allowed the assignment of all of the polypeptide backbone for switch I (in all six chains). Switch II is more flexible in this crystal form and a complete model could only be built in three or four copies of RAS per asymmetric unit. Further evidence for the flexibility of switch II is that chain A adopted a different conformation in this region owing to interactions with a symmetry-related molecule (Fig. 1*B*). The six chains are less sterically hindered than in other published RAS crystal structures, such as $KRAS_{188}^{G13D}$ (21) PDB ID code 4DST. The solvent channels are also much larger, facilitating compound diffusion; consequently, bound compounds have more freedom to be accommodated within $KRAS_{169}^{Q61H}$ crystals, and the structures are more likely to represent the interaction in solution. In addition, six independent protein chains are available for binding of compounds within the asymmetric unit, making this crystal form particularly suitable for compound-soaking experiments.

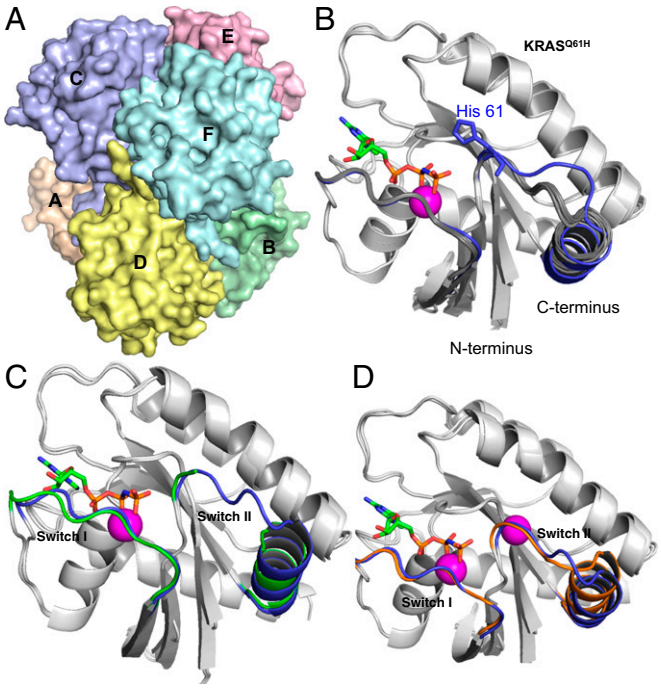

Fig. 1. $KRAS_{169}^{Q61H}$ structure analysis using new crystallization conditions. $KRAS_{169}^{Q61H}$ protein was crystallized with bound GTP-analog GppNHp. (*A*) Surface representation of the asymmetric unit containing the six $KRAS_{169}^{Q61H}$ proteins in different colors with different chains, labeled A–F. (*B*) Ribbon representation of $KRAS_{169}^{Q61H}$ showing an overlay of the six chains, of the asymmetric unit. The switch regions of five proteins (B–F) are identical (depicted in dark gray), and one (chain A) has a stabilized switch I and switch II (depicted in blue) due to interactions with neighboring protein molecules in the crystal lattice. Residue H61 and GppNHp are indicated and one Mg atom (shown as a magenta sphere) was identified per chain. *C* and *D* show ribbon representation overlays of the $KRAS_{169}^{Q61H}$ (chain A) structure with $KRAS_{188}^{G12V}$ (*C*, switch I and switch II depicted in green) and $KRAS_{188}^{G12D}$ (*D*, switch I and switch II depicted in brown), highlighting structural conservation across RAS mutations.

As a comparison with the $KRAS_{169}^{Q61H}$ crystals, we also determined crystal structures of WT $KRAS_{188}$, mutant $KRAS_{188}^{G12V}$ (*SI Appendix*, Fig. S2 and Table S2), and $KRAS_{188}^{G12D}$ (all isoform 4B) (*SI Appendix*, Fig. S3 and Table S2) with a GTP analog (GppNHp), using crystallization conditions similar to those described previously for full-length $KRAS_{188}^{G12D}$ (23). When the crystal packings of $KRAS_{169}^{Q61H}$ and $KRAS_{188}^{G12D}$ mutant proteins are compared, the switch regions are more solvent-accessible and less sterically hindered for the Q61H crystal. A further comparison was carried out between the switch regions of the two full-length KRAS structures (G12V and G12D) with our new $KRAS_{169}^{Q61H}$ structure (amino acids 1–169, Fig. 1 *C* and *D*). Both $KRAS_{169}^{Q61H}$ and $KRAS_{188}^{G12V}$ lack stabilization in the switch II region, and this instability could be attributed to the lack of a Mg ion binding to the switch II. All of the comparisons and observations between different crystal forms and mutants led us to conclude that the $KRAS_{169}^{Q61H}$ crystals were the best option for crystal-soaking experiments.

PPI-Net Fragment Screen with $KRAS_{166}^{G12V}$. We previously identified a compound series that binds to RAS in pocket I using a high-affinity anti-RAS intracellular antibody fragment in competition surface plasmon resonance (SPR) (28). In the present paper, we used direct screening of KRAS with a compound library using SPR. The library used was triaged for possible PPI inhibitors and comprised 1,534 compounds (the PP1-net screening collection). To identify specific KRAS binders, the library was simultaneously negatively screened against two control proteins, namely the LIM-only protein 2 (LMO2) and a fusion protein consisting of LMO2 bound by an intracellular antibody VH fragment (LMO2-VH fusion) (30). Responses were referenced by subtracting those measured against the control protein LMO2 from the responses measured against KRAS (R_{ref}). Compounds were selected as hits if R_{ref} was over 10 RU and if compounds did not bind the LMO2-VH fusion protein. Thirty compounds bound to $KRAS_{166}^{G12V}$ (*SI Appendix*, Fig. S4*A*) of which 7 showed RAS specificity. Four of these compounds were available in sufficient quantities (with identities confirmed by mass spectroscopy) to allow waterLOGSY NMR to be carried out showing that PPIN-1 and PPIN-2 (the chemical structures are shown in Fig. 2 *A* and *B*) have good interaction properties with $KRAS_{166}^{G12V}$-GppNHp (*SI Appendix*, Fig. S4 *A*–*C*). Furthermore, the two PPIN compounds still bind to KRAS in waterLOGSY experiments in the presence of the RAS-inhibitory single-chain variable region antibody fragment (scFv) as a competitor. Thus, in this orthogonal assay, PPIN-1 and -2 were confirmed to bind to $KRAS_{166}^{G12V}$, but neither compound was prevented from binding to KRAS by the anti-RAS scFv intracellular antibody fragment as shown using Bioluminescence Resonance Energy Transfer (BRET)-based RAS biosensors (31)

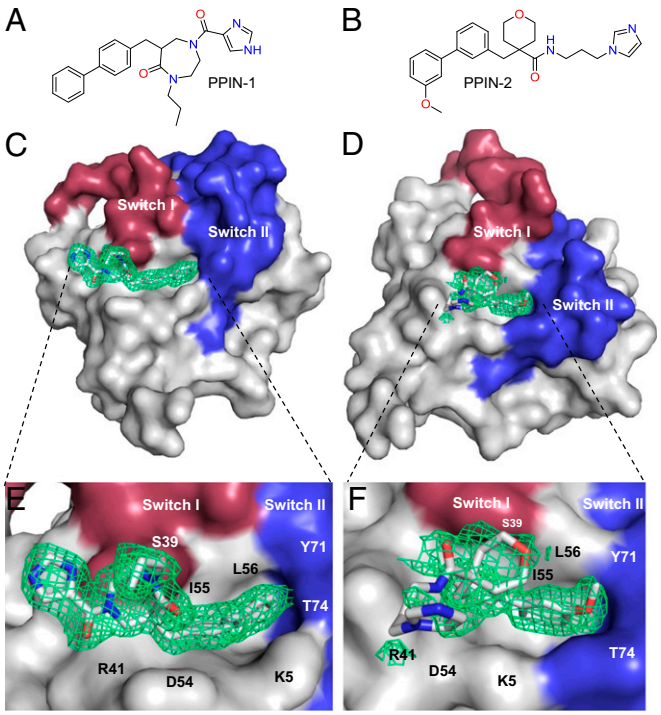

Fig. 2. Crystal structure of PPIN-1 and PPIN-2 bound to $KRAS_{169}^{Q61H}$-GppNHp. The crystal structure of $KRAS_{169}^{Q61H}$ with PPIN-1 and PPIN-2 was derived by crystal soaking with the compounds (their structures are shown in *A* and *B*, respectively). (*C* and *D*) Surface representations of the binding of PPIN-1 and PPIN-2 into pocket I close to the switch regions I (red) and II (blue). Good 2mFo-DFc electron density (green mesh) was found for the whole of PPIN-1 and for the biphenyl head group of PPIN-2 (green mesh) but less contiguous for the rest of the molecule. (*E* and *F*) Expanded views of the interactions of PPIN-1 and PPIN-2 with KRAS with the following residues in contact: K5, L6, V7, S39, Y40, R41, D54, I55, L56, Y71, and T74.

to assess intracellular RAS-protein interactions. As predicted from the waterLOGSY data using the intracellular antibody fragment, the PPIN compounds did not disrupt the interaction of $KRAS_{166}^{G12D}$ with the anti-RAS iDAb (VHY6) with a dematured version of the iDAb (VHY6dm) or with full-length CRAF ($CRAF^{FL}$) (*SI Appendix*, Fig. S4*D*). This discrepancy between in vitro affinity and in cell potency could be attributed to targets with high conformational variability (like RAS switch regions) interacting with allosteric binders (32, 33).

Crystal Soaking of $KRAS_{169}$Q61H with PPIN-1 and -2. We determined the RAS-binding sites of PPIN-1 and PPIN-2 by soaking $KRAS_{169}^{Q61H}$ crystals. Crystals of KRAS soaked with PPIN-1 diffracted to 1.63 Å (Fig. 2 *C* and *E* and *SI Appendix*, Table S3). Good electron density was observed for the ligand in one chain of the asymmetric unit (chain A, in which the switch regions are stabilized due to additional interactions on the opposite face with residues Arg102 and Lys101 from chain B in a neighboring asymmetric unit) and located adjacent to the C-terminal end of the switch I and switch II regions in pocket I. PPIN-1 primarily contacts $KRAS_{169}^{Q61H}$ with the biphenyl head group via van der Waals interactions. No hydrogen bonds are formed with the protein. Crystals soaked with PPIN-2 diffracted to 1.7 Å. For this compound, clear electron density corresponding to the methoxy-biphenyl anchor group was observed in four of the six chains (Fig. 2 *D* and *F*). Weaker electron density was observed around the linker and tail groups, suggesting that the rest of the compound remains flexible when bound to the protein. It was noteworthy that both PPIN compounds have the same biphenyl anchoring group but different tail functional groups, suggesting that the biphenyl-type groups of PPIN-1 and -2 are key in targeting these compounds to the pocket I-binding site.

Design and Characterization of RAS-Binding Cross-Over Compounds. Our data show that PPIN-1 and PPIN-2 bind to KRAS at the same pocket I as several previously identified compounds (23), but they do not disrupt RAS function. To understand the lack of RAS inhibition of the PPIN compounds, we selected one of our RAS-binding intracellular antibody-derived compounds (Abd-7) able to interfere with RAS PPI in cells (28). We used the computational chemistry suite FORGE (https://www.cresset-group.com/forge/; ref. 34) that employs a ligand comparison method to align and score molecules independently using their shape and electrostatic properties, aiding the understanding of structure–activity relationships. FORGE was used to compare the structures of PPIN-1 and -2 with Abd-7 by performing an alignment based on the surfaces of the compounds only and detected similarities in the lower half of the molecules (Fig. 3 *A* and *B*). The aromatic ring of the benzodioxane moiety in Abd-7 aligned with the terminal biphenyl aryl ring in both PPIN compounds, and the pyridine ring of Abd-7 aligned with the middle aromatic ring of both PPIN compounds. This suggested that the PPIN biphenyl system might act as the anchor to the RAS protein. The alignment with the functional groups on the upper half of the molecules was poor. We used these analyses to design of cross-over compounds linking the common diphenyl-anchoring moiety of PPIN-1 and PPIN-2 to the Abd-7 aniline fragment.

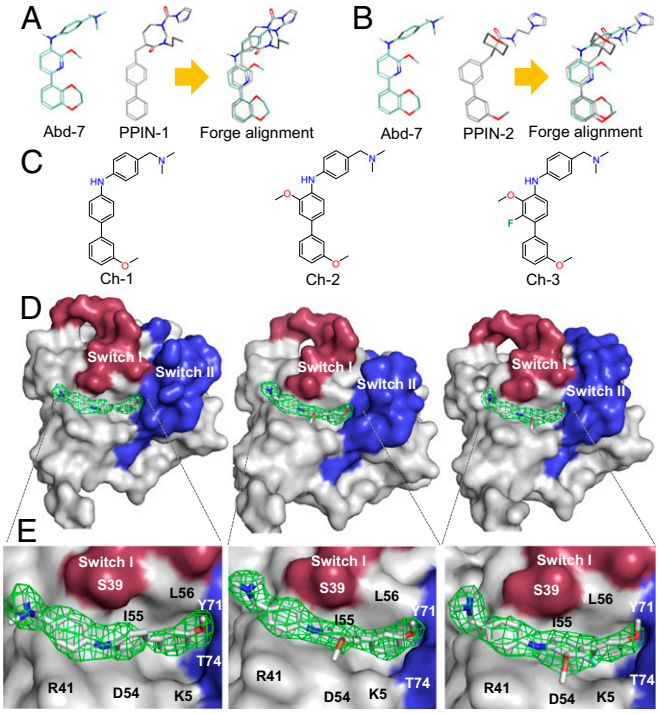

Fig. 3. Abd and PPI-net compound alignment and cross-over compound crystallography. Alignments were carried out with the computational chemistry suite FORGE. (*A*) Abd-7 and PPIN-1 with alignments. (*B*) Abd-7 and PPIN-2. Three cross-over compounds were synthesized after the alignments, which are shown in *C* (*Left*, Ch-1; *Middle*, Ch-2; *Right* Ch-3). These compounds were soaked into $KRAS_{169}^{Q61H}$-GppNHp crystals. (*D*) A surface representation of the binding of Ch-1 (*Left*), Ch-2 (*Middle*), and Ch-3 (*Right*) in KRAS pocket I, close to the switch regions I (red) and II (blue). Full electron density (2Fo-Fc) was found for the three compounds, all depicted as a green mesh. (*E*) An expanded view of the interaction of the compounds with KRAS with the following residues in contact: K5, L6, V7, S39, R41, R41, D54, I55, L56, Y71, and T74.

Three cross-over compounds (Fig. 3*C*: Ch-1, Ch-2, and Ch-3) were synthesized and their binding geometries were determined by X-ray crystallography using $KRAS_{169}^{Q61H}$ crystal soaking (Fig. 3 *D* and *E* and *SI Appendix*, Table S4). All three compounds showed very similar binding modes to Abd-7 with van der Waals contacts to K5, L6, V7, S39, Y40, R41, D54, I55, L56, G70, Y71, T74, and G75. Ch-1 was found in four of the six $KRAS_{169}^{Q61H}$ chains (A, B, C, and F); Ch-2 was again found in three of the six chains (A, B, and C) and Ch-3 was found in four of the six chains (A, B, C, and D). Thus, by combining the anchor constituent of the PPIN compounds with the aniline fragment of Abd-7, we generated a compound series showing good electron density for the entire molecule when bound to KRAS pocket 1.

The RAS-Binding Cross-Over Compounds Are PPI Inhibitors in Cells. The purpose of the compounds was to generate inhibitors of RAS PPI. The ability of the compounds to interfere with RAS-associated PPI was analyzed with our BRET-based RAS biosensor toolbox (31). The interaction of full-length $KRAS^{G12D}$ and either the anti-RAS iDAb VHY6, a dematured version of this iDAb (VHY6dm), or the natural RAS partner $CRAF^{FL}$ was assessed as a dose–response with the three compounds (respectively, Fig. 4 *A*–*C*). While the interaction of the high-affinity WT iDAb with RAS was minimally affected, even at the highest dose of compound (i.e., 20 μM), both the lower-affinity–dematured iDAb and CRAF binding to RAS were progressively impaired, starting at the lowest dose of 5 μM. No alteration in the BRET signal for the PPI of a non-relevant protein pair (LMO2-VH576dm) was observed (Fig. 4*D*), confirming that the dose–response effects of the Ch compounds was not due to loss of cell viability.

We also tested the effect of compound Ch-3 in the BRET assay using five different full-length $KRAS^{G12}$ mutations interacting with full-length CRAF (Fig. 4*E*: G12A, G12C, G12R, and G12V) or CRAF RAS-binding domain (RBD) (Fig. 4*G*: G12D). Each of these PPIs was inhibited by the Ch-3 compound in a dose–response assay. Furthermore, the BRET interaction signal between $KRAS^{G12D}$ and either PI3K (α or γ) or RALGDS was inhibited by Ch-3 (Fig. 4*G*), demonstrating that the BRET data are not restricted to KRAS-CRAF interaction. Finally, we show that Ch-3 interferes with NRAS and HRAS isoforms using the BRET biosensor assay. Interactions between full-length $NRAS^{Q61H}$ or $HRAS^{G12V}$ and full-length CRAF (Fig. 4*F*), between $NRAS^{Q61H}$ and RBD for PI3K (α or γ), CRAF, and RALGDS (Fig. 4*H*), or between $HRAS^{G12V}$ and RBD for PI3K (α or γ), CRAF, and RALGDS (Fig. 4*I*) are inhibited in the BRET assay by Ch-3.

These BRET data show that the three cross-over compounds can enter cells and reach their target protein (RAS) in the cytoplasmic environment. The BRET assay relies on cotransfected donor and acceptor expression plasmids, and we confirmed this inhibitory capability by testing the effect of the compounds on biomarker phosphorylation in DLD-1 colorectal cancer cells. The cells were incubated with our previously described antibody-derived compounds Abd-2 and Abd-7, the original PPIN-2 compound, or the three cross-over compounds Ch-1, -2, and -3. Phosphorylation of AKT (downstream of RAS-PI3K signaling) or phosphorylation of ERK (downstream of RAS-RAF signaling) was determined following EGF stimulation (Fig. 5 *A*–*C*). The PPIN-2 (and control Abd-2) had no effect on the levels of phospho-AKT or phospho-ERK even at 20 μM (addressed using Western blotting, Fig. 5 *A*–*C*), but we found that the three cross-over compounds caused loss of phospho-AKT or phospho-ERK, as did the previously described compound Abd-7. The most potent compound appears to be Ch-3, which invokes an almost complete reduction of phospho-AKT at a concentration of 10 μM while not affecting AKT protein levels (Fig. 5*C*).

The biomarker Western blotting assay was carried out 2.5 h after addition of the compounds, at which time no loss of viability was observed. The survival of DLD-1 cells was determined over 48- and 72-h periods using a dose–response (0–20 μM) (Fig. 5*D*; data shown at 72 h), allowing a calculation of IC_{50} for each compound (*SI Appendix*, Table S5). The previously characterized low-affinity Abd-2 compound does not affect DLD-1 viability over the range of concentrations nor does the PPIN-2 compound. Conversely, the intracellular antibody-derived compound Abd-7 causes loss of viability with IC_{50} of 10.8 μM at 48 h and 8.2 μM at 72 h. The potency of the two of the cross-over compounds (Ch-1 and Ch-3) is improved, relative to Abd-7, as these show IC_{50} at 72 h of 5.3 and 4.5 μM, respectively (*SI Appendix*, Table S5). This increased efficacy of Ch-3 in the challenge of DLD-1 viability matches the most efficacious compound in the signaling biomarker assay.

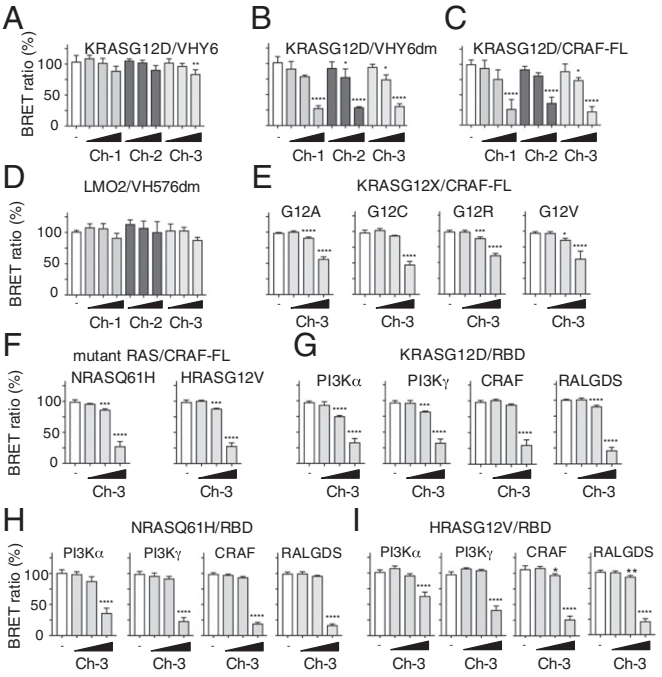

Fig. 4. Compound Ch-3 disrupts RAS-effector interactions. Assessment of the inhibition of RAS protein–protein interactions in cells by the chemical series compounds Ch-1, Ch-2, and Ch-3 using different BRET-based RAS biosensor expression vectors. (*A*–*C*) Data from BRET assays using RLuc8-$KRAS^{G12D}$ with either anti-RAS VHY6-GFP^2 (*A*) with dematured anti-RAS VHY6dm-GFP^2 (*B*) or with full-length $CRAF^{FL}$-GFP^2 (*C*). (*D*) Data from BRET assay using a negative control BRET-based biosensor LMO2/VH576dm. The VH576dm is a dematured anti-LMO2 VH. The data are computed relative to cells treated with DMSO vehicle only (open bar) or with Ch-1, Ch-2, or Ch-3 (shaded bars). (*E* and *F*) The effect of the Ch-3 compound on mutant $KRAS^{G12X}$ (*E*) and $NRAS^{Q61H}$ and $HRAS^{G12V}$ (*F*) interactions with $CRAF^{FL}$. (*G*–*I*) The effect of Ch-3 on the interaction of $KRAS^{G12D}$ (*G*), $NRAS^{Q61H}$ (*H*), and $HRAS^{G12V}$ (*I*) with various RAS effector domains (PI3Kα, PI3Kγ, CRAF, and RALGDS). The range of concentration of the compounds was 5, 10, and 20 μM. Each experiment was repeated at least twice (biological replicates). Statistical analyses were performed using a one-way ANOVA followed by Dunnett's posttests (*$P < 0.05$, **$P < 0.01$, ***$P < 0.001$, ****$P < 0.0001$). Error bars correspond to mean values ± SD of biological repeats. RLuc8-KRAS, NRAS, and HRAS all comprised full-length RAS components.

Discussion

The *RAS* family of genes is among the most frequently mutated in human cancer (e.g., up to 96% in pancreatic cancer) and therefore an important target for drug development. Targeting the RAS-effector PPI is one possible route to RAS inhibitors. Screening chemical compound libraries per se does not guarantee selection of compounds that will act as PPI inhibitors unless there is a method to guide the screen to functionally specific locations. Strategies are needed that will allow protein-binding compounds

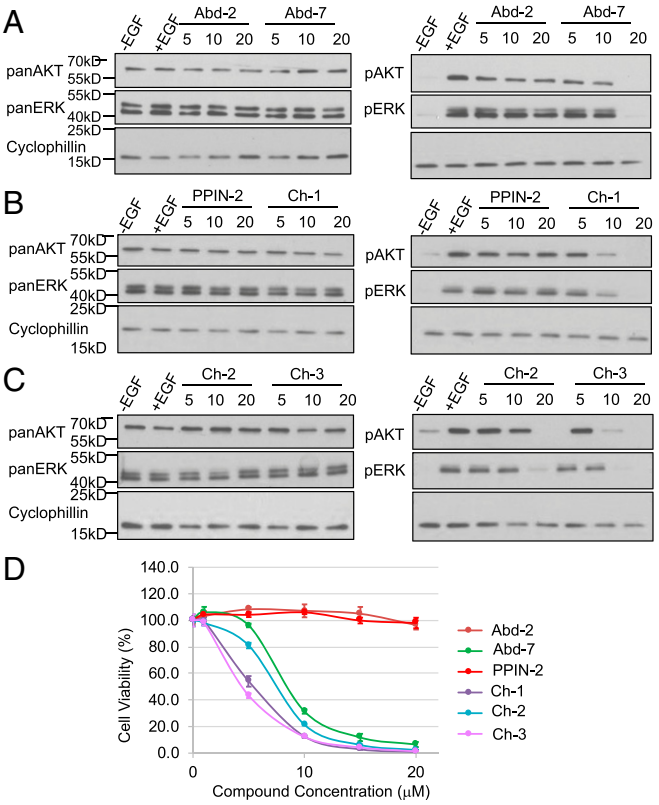

Fig. 5. Activity of compounds in a mutant KRAS human cancer cell. The new chemical series compounds Ch-1, -2, and -3 were assessed in two cell-based assays. (*A–C*) Western blot analysis of EGF-stimulated DLD-1 cells treated with 5, 10, and 20 μM of Abd-2 or Abd-7 (*A*), PPIN-2 or Ch-1 (*B*), and Ch-2 or Ch-3 (*C*). Cell extracts were fractionated by SDS/PAGE and transferred to PVDF membranes that were incubated with antibodies detecting the indicated proteins. These data are quantitated in *SI Appendix*, Fig. S5. (*D*) DLD-1 cell viability 72 h after treatment with a single application of compound at the indicated concentrations. Viability was determined using the CellTiter-Glo method and carried out in triplicate. The data are plotted as normalized cell viability mean with error bars showing SDs.

to be selected and improved in their properties related to the functional mechanism to be disrupted. In particular, X-ray crystallography of RAS proteins is a key method to determine the location and geometry of bound compounds. We optimized production of $KRAS_{169}^{Q61H}$ crystals for soaking of compounds for this purpose. It should be noted that these conditions, in principle, could be used to produce crystals of other RAS mutants suitable for compound-soaking experiments. Surface analysis of KRAS (using the CASTp server: sts.bioe.uic.edu/castp/) confirmed three pockets with internal volumes greater than 80 $Å^3$ (*SI Appendix*, Fig. S1*A*: pockets I, III, and IV) and a less deep, more like a shallow groove, pocket (*SI Appendix*, Fig. S1*A*: pocket II). Pocket I was previously identified in silico (29) and was also the site where DCAI was first selected (23). In addition, this pocket is close to the switch region and could act as a point of inhibition for PPI. Furthermore, we have focused on the identification and optimization of compounds inhibiting RAS-effector interactions and not other RAS modulation effects, such as DCAI has shown. Structural comparison of the six chains in the asymmetric unit show that compound binding has a minimal effect on the conformation of the switch regions in RAS protein. Any observed differences are no more than twice the coordinate error (35) and therefore cannot be considered significant. Comparison of the temperature factors between RAS molecules with compound bound and 3GFT (where no compound is present) show no evidence that compound binding results in significant reduction in flexibility of switch II relative to the rest of the molecule, suggesting that any stabilization of the switch regions by compound binding is, at most, slight. Therefore, we conclude that any inhibitory effect observed is due to a disruption of RAS-effector PPI rather than any other modulation of the RAS protein.

We have screened a chemical library that yielded two RAS-binding compounds (the PPINs) and have shown, by crystallography, that they bind to pocket I near to the effector binding sites. However, when these were tested in an orthogonal NMR waterLOGSY binding assay, their binding to $KRAS_{166}^{G12V}$ was not impaired by the presence of the anti-RAS intracellular antibody fragment, nor did they interfere with PPI using a cell-based BRET assay (*SI Appendix*, Fig. S4). Crystallography and medicinal chemistry was undertaken to improve the initial PPIN hits using structure-based design combining the crystal information and molecular fragments from two different chemical series, namely PPIN and the Abd series (28). The resulting crossover compounds illustrate that this strategy guided the conversion of the PPIN RAS-binding compounds to RAS PPI inhibitors in a series (compounds designated Ch-1–3). These compounds have a low molecular weight suitable for further medicinal chemistry to improve drug-like properties and with better ligand efficiencies than their progenitors (*SI Appendix*, Table S5). Furthermore, the compounds have also shown better cell viability results than their progenitors. Their low molecular weight makes them a better starting point for the development of RAS inhibitors based on this promising chemical series.

We have previously shown that the Abd chemical series affected RAF, RAL, and PI3K interactions with RAS (28) and, due to the similarities in binding mode and orientation of the Ch series with the Abd series, we expect the Ch compounds to have a similar range of profiles with other KRAS mutants and also with NRAS and HRAS isoforms. This was confirmed using various $KRAS^{G12}$ mutants and the $NRAS^{Q61H}$ and $HRAS^{G12V}$ mutants with four effector molecules in BRET assays.

This approach shows that compounds binding in pocket I are not necessarily able to inhibit RAS PPI, but synthetically linking components of two classes of RAS-binding compounds can generate new active molecules that inhibit PPI. It should also be noted that the presence of pocket I in nonmutated forms of RAS as well as in mutant RAS (*SI Appendix*, Fig. S1 *B–G*) presents a technical challenge for the development of anti-RAS drugs since these will bind to the pocket in WT-activated RAS as well as in mutant RAS. Development of methodologies for specific drug delivery could avoid drug interference with nonmutated RAS. Approaches such as Antibody-Drug Conjugates (ADC) offer one route to avoid drugs entering normal cells (reviewed in ref. 36) by targeting antigens expressed on tumors. While this, in turn, has difficulties, since few surface antigens are tumor-specific, surfaceome studies of tumors (37, 38) can find possible markers or pairs of markers that may be useful for mono- or bispecific ADCs. An alternative approach, based on structure–activity relationships, could be the development of compounds anchoring at pocket I and moving toward the nucleotide-binding region of RAS or perhaps linking the "unselective" but potent compounds identified in pocket I to those binding in pocket II.

In conclusion, our approach demonstrates the importance in drug development of combining assays for PPI with the identification of compounds that bind at important locations but not necessarily with PPI properties. Thus, compounds binding with good potency to the target but not showing any effect on PPI could be utilized in combination chemistry to create new chemical series. A combination of high-resolution crystallography from different chemical series with biophysical competition assays, such as using high-affinity antibody fragments, is thus a powerful way to identify hit compounds of interest in analogous

settings. It is also useful in the development of new chemical series, even when initial compounds are inactive, and should allow directed medicinal chemistry for drug development.

Methods

Detailed methods on protein expression and purification, SPR screening, NMR analysis, crystallography experiments, cell-based assays, and chemical experiments can be found in *SI Appendix, Methods*. The atomic coordinates have been deposited in the Protein Data Bank (39–47).

ACKNOWLEDGMENTS. We thank the beamline staff at station I02 at the Diamond Light Source (Didcot, UK); the ID30A-3 station at the European Synchrotron Radiation Facility (Grenoble, France); the Engineering and Physical Sciences Research Council-funded network, PPI-net (Grants EP/I037210/1 and EP/I037172/1); GlaxoSmithKline for making the PPI-net screening collection available; Prof. Andy Wilson for help with the PPI-net screening collection; and Dr. Matthias Ehebauer for help and input into discussions about the RAS protein structures. This work was supported by grants from the Wellcome Trust (Grants 099246/Z/12/Z and 100842/Z/12/Z); the Medical Research Council (Grant MR/J000612/1); and Bloodwise (Grant 12051).

1. Cox AD, Fesik SW, Kimmelman AC, Luo J, Der CJ (2014) Drugging the undruggable RAS: Mission possible? *Nat Rev Drug Discov* 13:828–851.
2. Prior IA, Lewis PD, Mattos C (2012) A comprehensive survey of Ras mutations in cancer. *Cancer Res* 72:2457–2467.
3. Simanshu DK, Nissley DV, McCormick F (2017) RAS proteins and their regulators in human disease. *Cell* 170:17–33.
4. Gutierrez L, Magee AI, Marshall CJ, Hancock JF (1989) Post-translational processing of p21ras is two-step and involves carboxyl-methylation and carboxy-terminal proteolysis. *EMBO J* 8:1093–1098.
5. Wittinghofer A, Nassar N (1996) How Ras-related proteins talk to their effectors. *Trends Biochem Sci* 21:488–491.
6. Bos JL, Rehmann H, Wittinghofer A (2007) GEFs and GAPs: Critical elements in the control of small G proteins. *Cell* 129:865–877.
7. Cherfils J, Zeghouf M (2013) Regulation of small GTPases by GEFs, GAPs, and GDIs. *Physiol Rev* 93:269–309.
8. Hunter JC, et al. (2015) Biochemical and structural analysis of common cancer-associated KRAS mutations. *Mol Cancer Res* 13:1325–1335.
9. Wood KW, Sarnecki C, Roberts TM, Blenis J (1992) Ras mediates nerve growth factor receptor modulation of three signal-transducing protein kinases: MAP kinase, Raf-1, and RSK. *Cell* 68:1041–1050.
10. Scott DE, Bayly AR, Abell C, Skidmore J (2016) Small molecules, big targets: Drug discovery faces the protein-protein interaction challenge. *Nat Rev Drug Discov* 15:533–550.
11. Spiegel J, Cromm PM, Zimmermann G, Grossmann TN, Waldmann H (2014) Small-molecule modulation of Ras signaling. *Nat Chem Biol* 10:613–622.
12. Whyte DB, et al. (1997) K- and N-Ras are geranylgeranylated in cells treated with farnesyl protein transferase inhibitors. *J Biol Chem* 272:14459–14464.
13. Tanaka T, Rabbitts TH (2008) Functional intracellular antibody fragments do not require invariant intra-domain disulfide bonds. *J Mol Biol* 376:749–757.
14. Tanaka T, Rabbitts TH (2012) Intracellular antibody capture (IAC) methods for single domain antibodies. *Methods Mol Biol* 911:151–173.
15. Cochet O, et al. (1998) Intracellular expression of an antibody fragment-neutralizing p21 ras promotes tumor regression. *Cancer Res* 58:1170–1176.
16. Dewhirst MW, Secomb TW (2017) Transport of drugs from blood vessels to tumour tissue. *Nat Rev Cancer* 17:738–750.
17. Ostrem JM, Shokat KM (2016) Direct small-molecule inhibitors of KRAS: From structural insights to mechanism-based design. *Nat Rev Drug Discov* 15:771–785.
18. Ledford H (2015) Cancer: The Ras renaissance. *Nature* 520:278–280.
19. Burns MC, et al. (2014) Approach for targeting Ras with small molecules that activate SOS-mediated nucleotide exchange. *Proc Natl Acad Sci USA* 111:3401–3406.
20. Lito P, Solomon M, Li LS, Hansen R, Rosen N (2016) Allele-specific inhibitors inactivate mutant KRAS G12C by a trapping mechanism. *Science* 351:604–608.
21. Maurer T, et al. (2012) Small-molecule ligands bind to a distinct pocket in Ras and inhibit SOS-mediated nucleotide exchange activity. *Proc Natl Acad Sci USA* 109:5299–5304.
22. Ostrem JM, Peters U, Sos ML, Wells JA, Shokat KM (2013) K-Ras(G12C) inhibitors allosterically control GTP affinity and effector interactions. *Nature* 503:548–551.
23. Sun Q, et al. (2012) Discovery of small molecules that bind to K-Ras and inhibit Sos-mediated activation. *Angew Chem Int Ed Engl* 51:6140–6143.
24. Winter JJ, et al. (2015) Small molecule binding sites on the Ras:SOS complex can be exploited for inhibition of Ras activation. *J Med Chem* 58:2265–2274.
25. Athuluri-Divakar SK, et al. (2016) A small molecule RAS-mimetic disrupts RAS association with effector proteins to block signaling. *Cell* 165:643–655.
26. Patricelli MP, et al. (2016) Selective inhibition of oncogenic KRAS output with small molecules targeting the inactive state. *Cancer Discov* 6:316–329.
27. Welsch ME, et al. (2017) Multivalent small-molecule Pan-RAS inhibitors. *Cell* 168:878–889.e29.
28. Quevedo CE, et al. (2018) Small molecule inhibitors of RAS-effector protein interactions derived using an intracellular antibody fragment. *Nat Commun* 9:3169.
29. Grant BJ, et al. (2011) Novel allosteric sites on Ras for lead generation. *PLoS One* 6:e25711.
30. Sewell H, et al. (2014) Conformational flexibility of the oncogenic protein LMO2 primes the formation of the multi-protein transcription complex. *Sci Rep* 4:3643.
31. Bery N, et al. (2018) BRET-based RAS biosensors that show a novel small molecule is an inhibitor of RAS-effector protein-protein interactions. *eLife* 7:e37122.
32. Johnstone S, Albert JS (2017) Pharmacological property optimization for allosteric ligands: A medicinal chemistry perspective. *Bioorg Med Chem Lett* 27:2239–2258.
33. Lawson ADG, MacCoss M, Heer JP (2018) Importance of rigidity in designing small molecule drugs to tackle protein-protein interactions (PPIs) through stabilization of desired conformers. *J Med Chem* 61:4283–4289.
34. Andersson V, et al. (2016) Macrocyclic prodrugs of a selective nonpeptidic direct thrombin inhibitor display high permeability, efficient bioconversion but low bioavailability. *J Med Chem* 59:6658–6670.
35. Cruickshank DWJ (1999) Remarks about protein structure precision. *Acta Crystallogr D Biol Crystallogr* 55:583–601.
36. Beck A, Goetsch L, Dumontet C, Corvaïa N (2017) Strategies and challenges for the next generation of antibody-drug conjugates. *Nat Rev Drug Discov* 16:315–337.
37. Town J, et al. (2016) Exploring the surfaceome of Ewing sarcoma identifies a new and unique therapeutic target. *Proc Natl Acad Sci USA* 113:3603–3608.
38. Martinko AJ, et al. (2018) Targeting RAS-driven human cancer cells with antibodies to upregulated and essential cell-surface proteins. *eLife* 7:e31098.
39. Cruz-Migoni A, et al. (2018) Structure-based development of new RAS-effector inhibitors from a combination of active and inactive RAS-binding compounds. Protein Data Bank. Available at https://www.rcsb.org/structure/6GOD. Deposited June 1, 2018.
40. Cruz-Migoni A, et al. (2018) Structure-based development of new RAS-effector inhibitors from a combination of active and inactive RAS-binding compounds. Protein Data Bank. Available at https://www.rcsb.org/structure/6GOE. Deposited June 1, 2018.
41. Cruz-Migoni A, et al. (2018) Structure-based development of new RAS-effector inhibitors from a combination of active and inactive RAS-binding compounds. Protein Data Bank. Available at https://www.rcsb.org/structure/6GOF. Deposited June 1, 2018.
42. Cruz-Migoni A, et al. (2018) Structure-based development of new RAS-effector inhibitors from a combination of active and inactive RAS-binding compounds. Protein Data Bank. Available at https://www.rcsb.org/structure/6GOG. Deposited June 1, 2018.
43. Cruz-Migoni A, et al. (2018) Structure-based development of new RAS-effector inhibitors from a combination of active and inactive RAS-binding compounds. Protein Data Bank. Available at https://www.rcsb.org/structure/6GOM. Deposited June 1, 2018.
44. Cruz-Migoni A, et al. (2018) Structure-based development of new RAS-effector inhibitors from a combination of active and inactive RAS-binding compounds. Protein Data Bank. Available at https://www.rcsb.org/structure/6GQT. Deposited June 8, 2018.
45. Cruz-Migoni A, et al. (2018) Structure-based development of new RAS-effector inhibitors from a combination of active and inactive RAS-binding compounds. Protein Data Bank. Available at https://www.rcsb.org/structure/6GQW. Deposited June 5, 2018.
46. Cruz-Migoni A, et al. (2018) Structure-based development of new RAS-effector inhibitors from a combination of active and inactive RAS-binding compounds. Protein Data Bank. Available at https://www.rcsb.org/structure/6GQX. Deposited June 5, 2018.
47. Cruz-Migoni A, et al. (2018) Structure-based development of new RAS-effector inhibitors from a combination of active and inactive RAS-binding compounds. Protein Data Bank. Available at https://www.rcsb.org/structure/6GQY. Deposited June 5, 2018.

PNAS
www.pnas.org

Supplementary Information for

Structure-based development of new RAS-effector inhibitors from a combination of active and inactive RAS-binding compounds.

Abimael Cruz-Migoni [1,2 ^], Peter Canning [1,3 ^], Camilo E. Quevedo [1 ^], Carole J.R. Bataille[4], Nicolas Bery [1], Ami Miller [1], Angela Russell [4], Simon E.V. Phillips [2,5], Stephen B. Carr[2,5], Terence H. Rabbitts [1, *]

* Email: terence.rabbitts@imm.ox.ac.uk

This PDF file includes:

Supplementary text (including compound experimental protocols and data)
Figures S1 to S6
Tables S1 to S5
References for SI citations

METHODS

Recombinant protein expression for crystallography

$KRAS_{169}^{Q61H}$, and $KRAS_{188}^{G12D}$ cDNAs were cloned into the pRK-172 vector using NdeI and BamHI restriction sites. Genes were placed in-frame with an N-terminal 6 x his-tag and the TEV protease recognition site. $KRAS_{188}^{WT}$ and $KRAS_{188}^{G12V}$ constructs were generated using QuikChange Site-Directed Mutagenesis kit (Agilent Technologies, USA) using pRK-172-$KRAS_{188}^{G12D}$ vector as a template. Plasmids containing pRK-172-6xHis-TEV-$KRAS_{169}^{Q61H}$, $KRAS_{188}^{G12D}$, $KRAS_{188}^{WT}$ or $KRAS_{188}^{G12V}$ sequences were transformed individually into B834(DE3)pLysS cells, which were grown in 25 ml LB medium with 50 µg/ml Carbenicillin and 34 µg/ml Chloramphenicol for 16 hours, before adding to 1L LB medium containing the same antibiotics. Protein expression was induced when cells reached an OD_{600} of 0.6 by addition of 1-thio-β-D-galactopyranoside (IPTG) to a final concentration of 0.5 mM followed by overnight incubation at 16°C. Bacteria were harvested by centrifugation (5180g, 30 mins, 4 °C) resuspended in 60 ml of 50 mM Tris-HCl, pH 7.5, 500 mM NaCl, 5 mM $MgCl_2$ and 10 mM imidazole also containing one EDTA-free protease inhibitor cocktail table (Roche Diagnostics, Mannheim, Germany). Cells were then lysed by sonication using five 30s pulses on power setting 16 with 1 min pauses on ice between pulses and insoluble debris removed by centrifugation (75,600g, 20 mins, and 4 °C). Supernatant was applied to nickel agarose beads (Invitrogen) by gravity, beads were then washed twice using same lysis buffer containing 50 mM imidazole and bound proteins were eluted in 50 mM Tris-HCl, pH 7.5, 500 mM NaCl, 5 mM $MgCl_2$ and 300 mM imidazole. For $KRAS_{188}^{G12D}$,$KRAS_{188}^{WT}$ and $KRAS_{188}^{G12V}$ HIS-tagged TEV protease (1.4mg/ml) was added at a ratio of 1:100 to the eluate and the sample dialysed against 50 mM Tris-HCl, pH 7.5, 500 mM NaCl, 5 mM $MgCl_2$, overnight at 4°C. His-tagged TEV protease and cleaved HIS-tag were removed by reapplication of the digestion to nickel agarose beads (Invitrogen). Samples containing RAS protein were concentrated using Vivapore 10/20 mL concentrator (7.5 kDa molecular weight cut-off; Sartorius Vivapore). The proteins were further purified by gel filtration using a Superdex 75 Increase 10/300 GL column (GE Healthcare, Uppsala, Sweden) equilibrated with 20 mM HEPES pH 8.0, 150 mM NaCl , 5 mM $MgCl_2$ and 1 mM DTT at a flow rate of 0.5 ml/min. Fractions corresponding to RAS were pooled and concentrated to 45-75 mg/ml for crystallization trials. Protein concentration was determined from a theoretical extinction coefficient at 280 nm calculated using ProtParam tool (https://web.expasy.org/protparam/). Protein purity was analyzed by SDS-PAGE stained with Instant Blue (Expedeon). The purification procedure of $KRAS_{188}^{G12D}$, $KRAS_{188}^{WT}$ or $KRAS_{188}^{G12V}$ proteins were the same as for the $KRAS_{166}^{G12V}$ and $KRAS_{169}^{Q61H}$ described above, except gel filtration used the following buffer (25 mM TrisCl, pH 8.0, 100 mM NaCl, 5 mM $MgCl_2$ and 1 mM TCEP). Nucleotide exchange for crystallographic samples was carried out following published procedures (1).

Protein crystallization and structure determination

$KRAS_{169}^{Q61H}$ crystals were grown at 4 °C by mixing 1.5 ul of protein (75 mg/ml) with an equal volume of crystallization buffer before equilibrating against 0.5 ml of crystallization buffer using sitting drop vapor diffusion. Crystal of this variant appeared in drops containing 8-15% w/v Polyethylene Glycol 3350 and 0.2 M lithium citrate pH 5.5. For $KRAS_{188}^{G12D}$ crystals, drops were prepared by mixing 1.5 µl of protein at 45 mg/ml with 1.5 µl of reservoir consisting of 0.1 M TrisCl pH 8.0, 0.2 M NaOAc and 30-35 % PEG 4000 in 24-well Cryschem sitting-drop plates. Crystals of $KRAS_{188}^{WT}$ and $KRAS_{188}^{G12V}$ mutants were obtained in a sitting-drop setup experiment using micro-seeding. $KRAS_{188}^{WT}$ protein and precipitant were mixed in a 1:1 ratio in an initial volume of 2 ul and 0.5 ul of $KRAS_{188}^{G12D}$ micro-crystals were added. $KRAS_{188}^{G12D}$ seed stocks were prepared by mechanical homogenization of crystals using the Seed Bead Kit (Hampton Research) as

described by Luft & DeTitta (2). Micro-crystals were suspended in 50µl reservoir solution containing the seed bead followed by mixing for 3min using a laboratory vortex. The seed-stock solutions were stored at −20°C The same procedure was followed for the generation of $KRAS_{188}^{G12V}$crystals. $KRAS_{188}^{G12V}$ and $KRAS_{166}^{WT}$ crystals were obtained in a crystallization solution of 0.1 M Tris pH 8.0, M NaOAc, 31.4% PEG 4000.
Prior to data collection, crystals were cryo-protected by addition of 20% glycerol to the crystallization buffer, then flash-cooled in liquid nitrogen. For crystal soaking experiments, compounds were added individually (25-50mM of compound in 100%DMSO, with a final DMSO concentration of 6-12% v/v) to the crystallization buffer. Crystals were then transferred to solution containing compound for a minimum of 5 mins. Soaked crystals were also cryo-protected with 20% glycerol and flash-cooled in liquid nitrogen for data collection. X-ray diffraction data were collected at either Diamond Light Source (DLS, Oxfordshire, UK) or European Synchrotron Radiation Facility (ESRF, Grenoble, France). The structure of $KRAS_{169}^{Q61H}$ GPPNHP and $KRAS_{188}^{G12D}$ GPPNHP were solved by molecular replacement using Protein Data Bank (PDB) codes 3GFT and 4DSU, respectively as a search models, within the program Phaser (3). $KRAS_{188}^{WT}$, $KRAS_{166}^{G12V}$ and $KRAS_{188}^{G12V}$ structures were again solved by molecular replacement using the $KRAS_{188}^{G12D}$ GPPNHP solved in this study as a search model. Structures were refined using REFMAC5 (4) and manually corrected using COOT (5). The refined models were validated using MOLPROBITY (6) and Phenix software packages (7) (8). Figures were created using PyMOL (DeLano, 2002). Data collection and refinement statistics are shown in Supplementary Tables 1-4.

Protein expression and purification for SPR fragment screen
The DNA sequence encoding human $KRAS_{166}^{G12V}$ (Uniprot P01116, isoform 4B, residues 1-166) was cloned into the vector pRK, modified to encode an N-terminal hexahistidine tag, TEV cleavage site and AviTag. The LMO2 and the LMO2-VH fusion cDNA were cloned into the vector pOPINS, modified to encode an N-terminal hexahistidine tag, SUMO tag and AviTag. Proteins were expressed in C41(DE3) or Lemo21 cells (NEB) using 0.5mM isopropyl 1-thio-β-D-galactopyranoside (IPTG) for overnight induction at 15ºC. Cells expressing LMO2 were supplemented with 0.1mM $ZnCl_2$. Harvested cells were re-suspended in binding buffer (50mM HEPES pH 7.5, 500mM NaCl, 5% glycerol, 10mM imidazole, 2mM 2-mercaptoethanol) supplemented with Complete Protease Inhibitors (Roche) and disrupted using a cell disruptor (Constant Systems) at 25kPSI, 5ºC. Proteins were partially purified by nickel affinity chromatography, eluting in 500mM imidazole. $KRAS_{166}^{G12V}$ protein was loaded with GppNHp as previously described (1). The N-terminal AviTags on all proteins were biotinylated by treatment with biotin ligase enzyme (BirA) overnight at 4ºC in the presence of ATP, $MgCl_2$ and D-biotin. The hexahistidine and SUMO tags were also cleaved from the LMO2 proteins using SUMO protease. The proteins were further purified by size-exclusion chromatography using either a HiLoad S200 16/600 column or HiLoad S75 16/600 column equilibrated in gel filtration buffer (10mM HEPES pH 7.5, 150mM NaCl, 1mM 2-mercaptoethanol) or PBS on an Akta Avant FPLC system (GE Healthcare).
GST-tagged $KRAS_{166}^{G12V}$ was expressed and purified as previously described REF.

SPR screening
Biotinylated LMO2, KRAS and LMO2-VH fusion were immobilized on a streptavidin chip (GE Healthcare) and the PPI-Net library compounds were passed over the three proteins at 150µM concentration. SPR experiments were carried out using a Biacore T200 instrument (GE Healthcare) at 10 °C to preserve the protein immobilised on the sensor surface. Biotinylated proteins were immobilised on a streptavidin-coated sensor chip (chip

SA, GE Healthcare). The surface was washed with 1M NaCl, 50mM NaOH before immobilising ~4000 response units (RU) of 1µM GppNHp-loaded $KRAS_{166}^{G12V}$ using the 'aim for' program. Control proteins were immobilized at RU level corresponding to an equal number of moles of protein on the sensor surface as 4000 RU of $KRAS_{166}^{G12V}$. In practice this equated to ~4000 RU of LMO2 as the molecular weight (MW) of LMO2 is very close to $KRAS_{166}^{G12V}$. Flow cell 1 was blocked by injecting 10mM biocytin over the surface for 5 minutes at 10µl/min and used as the reference channel. Immobilisation was carried out in HEPES running buffer (10mM HEPES pH 7.4, 150mM NaCl, 0.005% P20, 5mM MgCl2, 10µM $ZnCl_2$). Compound solutions were prepared by transferring 1.5µl PPI-Net stock compounds at 10mM in 100% DMSO into 96-well plates (Greiner) using a multichannel pipette. 98.5µl running buffer with 3.5% DMSO was added to yield a solution of 150µM compound in running buffer with 5% DMSO. Compound solutions were injected over all 4 flow channels for 30 seconds at 30µl/min and dissociation monitored for 60 seconds. A negative control of running buffer with 5% DMSO was run after every 24 cycles. Between injections the flow system was washed with a solution of 50% DMSO. A solvent correction curve was used to correct for the effects of DMSO. Data were referenced, solvent corrected and processed using the T200 evaluation software. Single-point binding levels were exported to Excel. Data were baseline-corrected using the negative control binding levels as a reference and then binding levels measured against $KRAS_{166}^{G12V}$ plotted against binding levels measured against the control proteins. Hit compounds were tested using X-ray crystallography. PPIN-1 and PPNI-2 gave clear electron density in X-ray crystallography.

Recombinant protein expression for NMR

$KRAS_{166}^{G12V}$ was cloned and isolated the same way as described in the recombinant protein expression for crystallization. $KRAS_{166}^{G12V}$ cDNA was cloned into the pGEX vector in-frame with an N-terminal Glutathione-S transferase (GST) tag. pGEX-GST-$KRAS^{G12V}$ was transformed into *E.coli* BL21 (DE3) cells. Bacterial cells were cultured at 37°C to an OD_{600} of 0.5 and induced with IPTG (isopropyl 1-thio-beta-D-galactopyranoside, final concentration 0.1mM) at 16°C overnight. The bacteria cultures were harvested by centrifugation and the cell pellets re-suspended in 50 mM Tris-HCl pH8.0, 140 mM NaCl, 1 mM mercaptoethanol supplemented with complete protease inhibitor (Roche). The GST-fusion proteins were purified by glutathione-sepharose column chromatography (GE Healthcare) and eluted with 50 mM Tris-HCl pH8.0, 10 mM reduced glutathione, 1 mM mercaptoethanol, 5 mM $MgCl_2$.

$KRAS_{166}^{G12V}$ protein samples were concentrated using Vivapore 10/20 mL concentrator (7.5 kDa molecular weight cut-off; Sartorius Vivapore) to a final volume of approximately 2 mL. RAS proteins were further purified by gel filtration on a HiLoad Superdex 75 10/300GL column (GE Healthcare) in a buffer containing 10 mM PBS pH 7.4, 5 mM $MgCl_2$ at a flow rate of 0.5 mL/min. Protein concentration was determined by extinction coefficient (ε_{280} = 54780 $M^{-1}cm^{-1}$). Protein purity was analysed by SDS-PAGE stained with Coomassie Brilliant Blue. Nucleotide exchange for crystallographic samples was carried out following published procedures (1)

NMR spectroscopy

NMR spectra were recorded on Bruker Avance spectrometers (AVII400 or AVIII400) in the deuterated solvent stated. The field was locked by external referencing to the relevant deuteron resonance. Chemical shifts (δ) are reported in parts per million (ppm) referenced to the solvent peak. The multiplicity of each signal is indicated by: s (singlet); br. s (broad singlet); d (doublet); t (triplet); dd (doublet of doublets); tt (triplet of triplets); or m (multiplet).

The number of protons (n) for a given resonance signal is indicated by nH. Coupling constants (J) are quoted in Hz and are reported to the nearest 0.1 Hz.

WaterLOGSY experiments

WaterLOGSY experiments (9) were conducted at a ^{1}H frequency of 600 MHz using a Bruker Avance spectrometer equipped with a BBI probe. All experiments were conducted at 298 K. 3 mm diameter NMR tubes with a sample volume of 200 µL were used in all experiments. Solutions were buffered using an H_2O PBS buffer corrected to pH 7.4 and 5mM $MgCl_2$. The sample preparation is exemplified as follows, the compound (10 µL of a 10 nM solution in DMSO-d_6) was added to an eppendorf before sequential addition of the H_2O PBS buffer (163.6 µL), D_2O (20 µL), and His-$KRAS_{166}^{G12V}$-GppNHP loaded protein (6.4 µL, 311.8 µM). The resulting solution was spun to ensure full mixing and transferred to a 3 mm NMR tube before the run. For a competition experiment using Y6-ScFv VH, the preparation was carried out in a similar manner; the compound (10 µL of a 10 nM solution in DMSO-d_6) was added to an eppendorf before sequential addition of the H_2O PBS buffer (146.4 µL), D_2O (20 µL), protein (6.4 µL, 311.8 µM) and Y6-ScFv (17.2 µL, 116.6 µM). The resulting solution was spun and transferred to a 3 mm NMR tube before the run. Negative controls (compound alone, without the protein) were prepared in a similar manner, in order to obtain an end volume of 200 µL.

FORGE Analysis

Alignments of the selected compounds were performed following the wizard menu in FORGE (http://www.cresset-group.com/forge/ (10)). Mol2 files of the Abd7 file was uploaded as the reference molecule. The protonation state for each molecule was selected by FORGE. Mol2 files for the selected molecules to be aligned were uploaded in the program (PPIN-1 and PPIN2). No other parameters were uploaded in the program until the selection for the results quality window appeared. For simplicity, no field alignments were used, only alignments from the compounds surfaces were selected from the highest score solutions to illustrate the results.

Chemical synthesis and characterization

All solvents and reagents were used as supplied (analytical or HPLC grade) without prior purification. Water was purified by an Elix® UV-10 system. Brine refers to a sat. aq. solution of sodium chloride. *In vacuo* refers to the use of a rotary evaporator attached to a diaphragm pump. Thin layer chromatography was performed on aluminium plates coated with 60 F254 silica. Plates were visualised using UV light (254 nm) or 1% aq. $KMnO_4$. Flash column chromatography was performed on Kieselgel 60M silica in a glass column. NMR spectra were recorded on Bruker Avance spectrometers (AVII400, AVIII 400, AVIIIHD 600 or AVIII 700) in the deuterated solvent stated. The field was locked by external referencing to the relevant deuteron resonance. Chemical shifts (δ) are reported in parts per million (ppm) referenced to the solvent peak. ^{1}H spectra reported to two decimal places, and ^{13}C spectra reported to one decimal place, and coupling constants (*J*) are quoted in Hz (reported to one decimal place). The multiplicity of each signal is indicated by: s (singlet); br. s (broad singlet); d (doublet); t (triplet); q (quartet); dd (doublet of doublets); td (triplet of doublets); qt (quartet of triplets); or m (multiplet). Low-resolution mass spectra were recorded on an Agilent 6120 spectrometer from solutions of MeOH. Accurate mass measurements were run on either a Bruker MicroTOF internally calibrated with polyalanine, or a Micromass GCT instrument fitted with a Scientific Glass Instruments BPX5 column (15 m x 0.25 mm) using amyl acetate as a lock mass, by the mass spectrometry department of the Chemistry Research Laboratory, University of Oxford, UK.; m/z values are reported in Daltons.

NMR spectra for the compounds are shown in Figure S6.

General procedure A

The requisite halogen (600 mg, 2.79 mmol, 1.0 eq.), K_2CO_3 (1.16 g, 8.37 mmol, 3.0 eq.), the requisite boronic acid (572 mg, 3.07 mmol, 1.1 eq.), and $Pd(dppf)Cl_2$ (100 mg, 0.140 mmol, 5 mol%) were added sequentially to a microwave vial equipped with a magnetic stirrer bar. The reaction vessel was fitted with a rubber septum and purged with N_2 for 5 min, before addition of a degassed solution of 1,4-dioxane/water (5:1, 8 mL) *via* syringe. The vial was then sealed and the reaction heated to 100 °C for 18 h. The mixture was cooled down, diluted with EtOAc (30 mL), and washed with a 50/50 solution of water and brine (2 x 30 mL). The organic phase was dried (Na_2SO_4) and concentrated *in vacuo.* Purification by column chromatography on silica gel (solvents as stated) afforded the desired product.

General procedure B

The requisite halogen (75 mg, 0.272 mmol, 1.0 eq.), Cs_2CO_3 (266 mg, 0.866 mmol, 3.0 eq.), the requisite amine (53 mg, 0.354 mmol, 1.3 eq.), XPhos (13 mg, 0.027 mmol, 10 mol%) and $Pd(OAc)_2$ (3 mg, 0.014 mmol, 5 mol%) were added sequentially to a microwave vial equipped with a magnetic stirrer bar. The reaction vessel was fitted with a rubber septum and purged with N_2 for 5 min, before addition of a degassed solution of 1,4-dioxane (3 mL) *via* syringe. The vial was then sealed and the reaction heated to 100 °C for 24 h. The mixture was cooled down, diluted with EtOAc (30 mL), and washed with a 50/50 solution of water and brine (2 x 30 mL). The organic phase was dried (Na_2SO_4) and concentrated *in vacuo.* Purification by column chromatography on silica gel (solvents as stated) afforded the desired product.

4'-chloro-3-methoxy-1,1'-biphenyl (1)

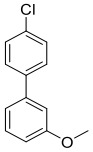

Following **General Procedure A**, 3-bromoanisole (200 mg, 1.07 mmol) and 4-chlorobenzylboronic acid (185 mg, 1.18 mmol) afforded the title product **1** (231 mg, 99%) as a clear oil that solidified on standing after purification on silica gel (EtOAc:pentane (1:99)).

^{1}H NMR (400 MHz, $CDCl_3$) δ = 7.52 (2H, dd, *J* 8.8, 0.7), 7.41 (2H, dd, *J* 8.8, 0.7), 7.36 (1H, dd, *J* 7.6, 0.7), 7.15 (1H, dquin, *J* 7.6, 0.7), 7.09 (1H, dt, *J* 2.6, 1.4), 6.92 (1H, ddt, *J* 8.3, 2.4, 1.0), 3.88 (3H, s); ^{13}C NMR (75 MHz, $CDCl_3$) δ = 160.0, 141.5, 139.5, 133.5, 129.9, 128.9, 128.4, 119.5, 112.9, 112.8, 55.3; LRMS (ESI+) 219.1 $(M+H)^+$.

***N*-(4-((dimethylamino)methyl)phenyl)-3'-methoxy-[1,1'-biphenyl]-4-amine (Ch-1)**

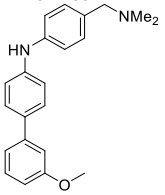

Following **General Procedure B**, **A** (155 mg, 0.711 mmol) and 4-amino-*N*,*N*-dimethylbenzylamine (128 mg, 0.853 mmol) afforded the title product **Ch-1** (209 mg, 88%)

as a yellow oil that solidified on standing after purification on silica gel (MeOH:CH_2Cl_2 (1:9)).
^{1}H NMR (600 MHz, MeOD) δ = 7.50 (2H, d, *J* 8.4), 7.30 (1H, t, *J* 8.0), 7.20 (2H, d, *J* 8.3), 7.16 (2H, d, *J* 8.4), 7.15 (2H, d, *J* 8.8), 7.11 (2H, d, *J* 8.3), 6.83 (1H, dd, *J* 8.3, 2.4), 3.84 (3H, s), 3.51 (2H, s), 2.32 (6H, s), NH was not observed; ^{13}C NMR (125 MHz, MeOD) δ = 161.7, 145.0, 144.7, 134.3, 132.1, 130.9, 129.1, 128.8, 119.8, 118.7, 118.3, 113.1, 113.0, 64.3, 55.8, 44.8; LRMS (ESI+) 333.1 $(M+H)^+$; HRMS (ESI^+) [$C_{22}H_{25}N_2O$] requires 333.4550, found 333.4538;

4-chloro-3,3'-dimethoxy-1,1'-biphenyl (2)

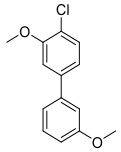

Following **General Procedure A**, 3-bromoanisole (200 mg, 1.07 mmol) and 4-chloro-3-methoxyphenyl boronic acid (220 mg, 1.18 mmol) afforded the title product **2** (232 mg, 99%) as a beige solid after purification on silica gel (EtOAc:pentane (1:99)).
^{1}H NMR (600 MHz, $CDCl_3$) δ = 7.42 (1H, dd, *J* 7.7, 0.7), 7.37 (1H, t, *J* 7.9), 7.16 (1H, dt, *J* 7.6, 0.9), 7.13 (1H, s), 7.11 (1H,ddd, *J* 11.4, 9.5, 2.0), 7.10 (1H, t, *J* 2.4), 6.93 (1H, dd, *J* 8.3, 2.6), 3.98 (3H, s), 3.88 (3H, s); ^{13}C NMR (125 MHz, $CDCl_3$) δ = 160.0, 155.1, 141.9, 141.2, 130.3, 129.9, 121.8, 120.1, 119.8, 113.1, 112.8, 111.1, 56.2, 55.4; LRMS (ESI+) 249.7 $(M+H)^+$.

***N*-(4-((dimethylamino)methyl)phenyl)-3,3'-dimethoxy-[1,1'-biphenyl]-4-amine (Ch-2)**

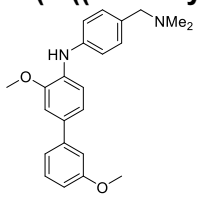

Following **General Procedure B**, **2** (185 mg, 0.746 mmol) and 4-amino-*N*,*N*-dimethylbenzylamine (134 mg, 0.895 mmol) afforded the title product **Ch-2** (226 mg, 91%) as a yellow oil after purification on silica gel (MeOH:CH_2Cl_2 (1:9)).
^{1}H NMR (600 MHz, MeOD) δ = 7.30 (1H, t, *J* 7.9) 7.29 (1H, d, *J* 7.9), 7.20 (2H, d, *J* 8.4), 7.18 (1H, d, *J* 2.0), 7.17 (1H, ddd, *J* 7.7, 1.7, 0.9), 7.14-7.12 (4H, m), 6.84 (1H, ddd, *J* 8.3, 2.6, 0.9), 3.94 (3H, s), 3.83 (3H, s), 3.47 (2H, s), 2.29 (6H, s), NH was not observed; ^{13}C NMR (125 MHz, MeOD) δ = 161.7, 151.0, 144.6, 144.2, 134.9, 133.8, 132.0, 130.9, 129.7, 120.4, 120.1, 118.9, 117.1, 113.4, 113.0, 110.9, 64.4, 58.4, 55.9, 44.9; LRMS (ESI+) 333.1 $(M+H)^+$; HRMS (ESI^+) [$C_{23}H_{27}N_2O_2$] requires 363.4810, found 363.4821.

4-chloro-2-fluoro-3,3'-dimethoxy-1,1'-biphenyl (3)

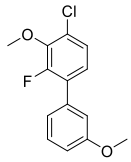

Following **General Procedure A**, 3-bromoanisole (200 mg, 1.07 mmol) and 4-chloro-2-fluoro-3-methoxyphenylboronic acid (241 mg, 1.18 mmol) afforded the title product **3** (272 mg, 96%) as a yellow oil after purification on silica gel (EtOAc:pentane (1:99)).
^{1}H NMR (600 MHz, $CDCl_3$) δ = 7.38 (1H, t, *J* 7.8), 7.22 (1H, dd, *J* 8.4, 1.8), 7.10 (1H, dd, *J* 8.6, 7.6), 710-7.09 (1H, m), 7.06 (1H, dd, *J* 2.7, 1.5), 6.95 (1H, ddd, *J* 8.3, 2.4, 1.0), 4.01 (3H, d, *J* 1.0), 3.86 (3H, s); ^{19}F NMR (565 MHz, $CDCl_3$) δ = -132.4 (d, *J* 8.0); ^{13}C NMR (125 MHz, $CDCl_3$) δ =159.6, 154.4, 152.7, 144.8 (d, *J* 14.3), 136.0, 129.5, 129.3 9d, *J*

13.2), 127.5 (d, *J* 2.2), 125.1 (d, *J* 3.3), 124.8 (d, *J* 3.3), 121.3 (d, *J* 2.2), 114.6 (d, *J* 2.2), 113.6, 61.6 (d, *J* 4.4), 55.3; LRMS (ESI+) 267.7 $(M+H)^+$.

_N_-(4-((dimethylamino)methyl)phenyl)-2-fluoro-3,3'-dimethoxy-[1,1'-biphenyl]-4-amine (Ch-3)

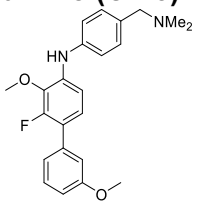

Following **General Procedure B**, **3** (110 mg, 0.414 mmol) and 4-amino-*N*,*N*-dimethylbenzylamine (75 mg, 0.497 mmol) afforded the title product **Ch-3** (226 mg, 91%) as a yellow oil after purification on silica gel ($MeOH:CH_2Cl_2$ (1:9)).

^1H NMR (600 MHz, MeOD) δ = 7.31 (1H, t, *J* 8.0), 7.24 (2H, d, *J* 8.3), 7.17 (2H, d, *J* 8.3), 7.08 (2H, td, *J* 8.6, 1.1), 7.05-7.03 (2H, m), 6.88 (1H, ddd, *J* 8.3, 2.6, 0.8), 3.91 (3H, d, *J* 0.9), 3.82 (3H, s), 3.49 (2H, s), 2.29 (6H, s), NH was not observed; ^{19}F NMR (565 MHz, MeOD) δ = -137.7 (d, *J* 8.2); ^{13}C NMR (125 MHz, MeOD) δ = 161.3, 155.1 (d, *J* 243.2), 143.7, 139.4 9d, *J* 4.4), 138.8, 138.6 (d, *J* 14.3), 132.0, 131.0, 130.5, 125.6 (d, *J* 4.4), 122.6 (d, 12.1), 122.3 (d, *J* 3.3), 120.1, 115.6 (d, *J* 3.3), 113.6, 112.3 (d, *J* 2.2), 64.4, 61.8 (d, *J* 4.4), 55.9, 45.0; LRMS (ESI+) 381.3 $(M+H)^+$; HRMS (ESI^+) [$C_{23}H_{26}FN_2O_2$] requires 381.4714, found 381.4702.

Tissue culture

HEK293T and DLD-1 cells and were grown in DMEM, high glucose, GlutaMax™ medium (Life Technologies) supplemented with 10% FBS (Sigma) and 1% Penicillin/Streptomycin (Life Technologies). Cells were grown at 37°C with 5% CO_2. The KRAS genotype in DLD-1 cells (heterozygous for $KRAS^{G13D}$/KRAS wild type) was confirmed by RNA analysis and sequencing (11).

BRET bioassay

The BRET-based RAS biosensors are built by fusing a donor molecule, a variant of the *Renilla* Luciferase (RLuc8), to full-length mutant RAS ($KRAS^{G12A}$, $KRAS^{G12C}$, $KRAS^{G12D}$, $KRAS^{G12V}$, $KRAS^{G12R}$, $NRAS^{Q61H}$ and $HRAS^{G12V}$ mutants) and an acceptor molecule, GFP^2, to RAS binders (iDAb RAS) or RAS effectors (full-length CRAF; PI3Kα, PI3Kγ, CRAF RBDs and RALGDS RA) (11). A BRET signal (or BRET ratio) occurs only when the donor (e.g. RLuc8-$KRAS^{G12D}$) and acceptor (e.g. GFP^2-$CRAF^{FL}$) molecules are in close proximity (≤ 10 nm). A competition assay involves the addition of a competitor (i.e. anti-RAS compounds) and is used to determine whether an inhibitor can interfere with RAS protein-protein interactions (PPIs). If the compounds impede RAS PPIs, a BRET signal decreased is monitored; otherwise the BRET signal is unchanged.

The BRET assay was performed as described in detail elsewhere (11). Briefly, 650,000 HEK293T cells were transfected with donor plasmid (RLuc8-mutant RAS) and acceptor plasmids (fusions of RAS binders/effectors with GFP^2) to allow the assessment of inhibitors of RAS-effector interaction. The transfection was carried out using Lipofectamine 2000 transfection reagent (Thermo-Fisher). Cells were detached 24 hours later and washed with PBS and seeded in a white 96 well plate (clear bottom, PerkinElmer, cat#6005181) in OptiMEM no phenol red medium (Life Technologies) supplemented with 4% FBS. Cells were left for 4 hours at 37 °C before adding compounds. 10 mM stock compounds in 100% DMSO were diluted in OptiMEM no red phenol + 4% FBS to reach 10X the final concentration (2% DMSO for each concentration). The final concentrations in the cells were 0, 5, 10 and 20 μM (with final 0.2% DMSO each). Quadruplicates were

performed for each point. Cells were left for an additional 20 hours at 37 °C before the BRET2 signal reading directly after addition of Coelenterazine 400a substrate (10 μM final) to cells (Cayman Chemicals, cat#16157). BRET2 reading was done on an Envision instrument (2103 Multilabel Reader, PerkinElmer) with the BRET2 Dual Emission optical module (515 nm ± 30 and 410 nm ± 80; PerkinElmer) or with a CLARIOstar instrument. The BRET ratio corresponds to the light emitted by the GFP^2 acceptor constructs (515 nm ± 30) upon addition of Coelenterazine 400a divided by the light emitted by the RLuc8 donor constructs (410 nm ± 80) with subtraction of the background (same ratio but with RLuc8 construct alone transfected in cells). The normalized BRET ratio is the BRET ratio normalized to the DMSO negative control and calculated as follows: ($BRET_{compound}$ / $BRET_{DMSO}$) x 100, where $BRET_{compound}$ correspond to the BRET ratio for the compound-treated cells, $BRET_{DMSO}$ to the DMSO-treated cells. Each experiment was repeated at least twice.

Quantification and statistical analysis

Statistical analyses of the BRET assays were performed using a one-way ANOVA followed by Dunnett's post-tests (*P<0.05, **P<0.01, ***P<0.001, ****P<0.0001) using GraphPad Prism 7 software.

Biomarker Western blot assay

DLD-1 cells were seeded at 4.5 x 10^5 cells per well in 6-well plates and incubated overnight. The media was aspirated and the cells were washed twice with PBS, before 2ml of serum free DMEM was added to the cells, which were incubated for a further 24 hours. The following day the media was replaced with compound containing media (0-20uM compound, with 0.2% DMSO) and the cells were incubated under culture conditions for 2.5 hours. The cells were stimulated with 50 ng/ml EGF for 10 min at 37°C. The cells were washed with cold PBS and were lysed using RIPA buffer (50mM Tris, pH 8.0, 150 mM NaCl, 1% Triton X-100, 0.5% sodium deoxycholate, 0.1% SDS) containing 1 mM DTT, Complete™ EDTA-free protease inhibitor and PhosSTOP™ (Roche). Cell lysates were sonicated using a Bioruptor® Pico Sonication System (Diagenode) and the protein concentration of each sample was quantified using the Pierce BCA Protein Assay Kit (Thermo Fisher Scientific). 10ug of protein was electrophoresed on a 12% Bis-Tris gel and bands were subsequently transferred to a Amersham™ Hybond® P 0.45 μm PVDF membranes (GE Healthcare). The membranes were blocked with 10%-BSA-TBST or 5%-milk-TBST before being incubated overnight at 4°C with appropriate antibodies (anti-phospho-p44/22 MAPK (ERK1/2) (1/5000, CST, 9101S), anti-p44/42 MAPK (total ERK1/2) (1/1000, CST, 9102S), anti-phospho-AKT S473 (1/2000, CST, 4058S), anti-AKT (1/2000, CST, 9272S), anti-cyclophilin B (1/1000, Abcam, 178397)). The membranes were washed with TBST and incubated with anti-rabbit IgG HRP-linked (1/2500, CST, 7074S) secondary antibody for 2 hours at room temperature. Following thorough washing the membranes were developed using Pierce™ ECL Western Blotting Substrate (Thermo Fisher Scientific) and CL-XPosure™ films (Thermo Fisher Scientific).

Cell viability assays

DLD-1 cells were seeded in culture media at 10,000 cells per well in ViewPlates-96 microplates (PerkinElmer) and allowed to adhere overnight at 37 °C, 5% CO_2. 10mM stock compounds, solubilised in DMSO, were diluted in culture media at final concentrations ranging from 0-20μM, each containing 0.2% DMSO. The media on the cells was removed and 100ul of the compound containing media was added. Quadruplicates were set up for each compound concentration. The cells were incubated under standard culture

conditions for a further 72 hours. Cellular viability was assessed using the CellTiterGlo Luminescent Cell Viability Assay (Promega) according to the manufacturers' instructions. CellTiterGlo was added (50% v/v) to the cells, and the plates incubated for 10 minutes prior to luminescent detection using an Envision 2103 Multilable Microplate Reader (PerkinElmer). The luminescence signals obtained from the compound treated cells were normalized against the signal obtained for the DMSO-only treated cells. The IC_{50} values were generated by non-linear regression using GraphPad Prism 7 software (GraphPad Inc).

PDB files

$KRAS_{188}^{WT}$ GppNHp	**PDB ID: 6GOD**
$KRAS_{188}^{G12V}$ GppNHp	**PDB ID: 6GOE**
$KRAS_{188}^{G12D}$ GppNHp	**PDB ID: 6GOF**
$KRAS_{169}^{Q61H}$ GppNHp	**PDB ID: 6GOG**
$KRAS_{169}^{Q61H}$ GppNHp-PPIN-1	**PDB ID: 6GOM**
$KRAS_{169}^{Q61H}$ GppNHp-PPIN-2	**PDB ID: 6GQT**
$KRAS_{169}^{Q61H}$ GppNHp-Ch-1	**PDB ID: 6GQW**
$KRAS_{169}^{Q61H}$ GppNHp-Ch-2	**PDB ID: 6GQX**
$KRAS_{169}^{Q61H}$ GppNHp-Ch-3	**PDB ID: 6GQY**

Suplementary Figures

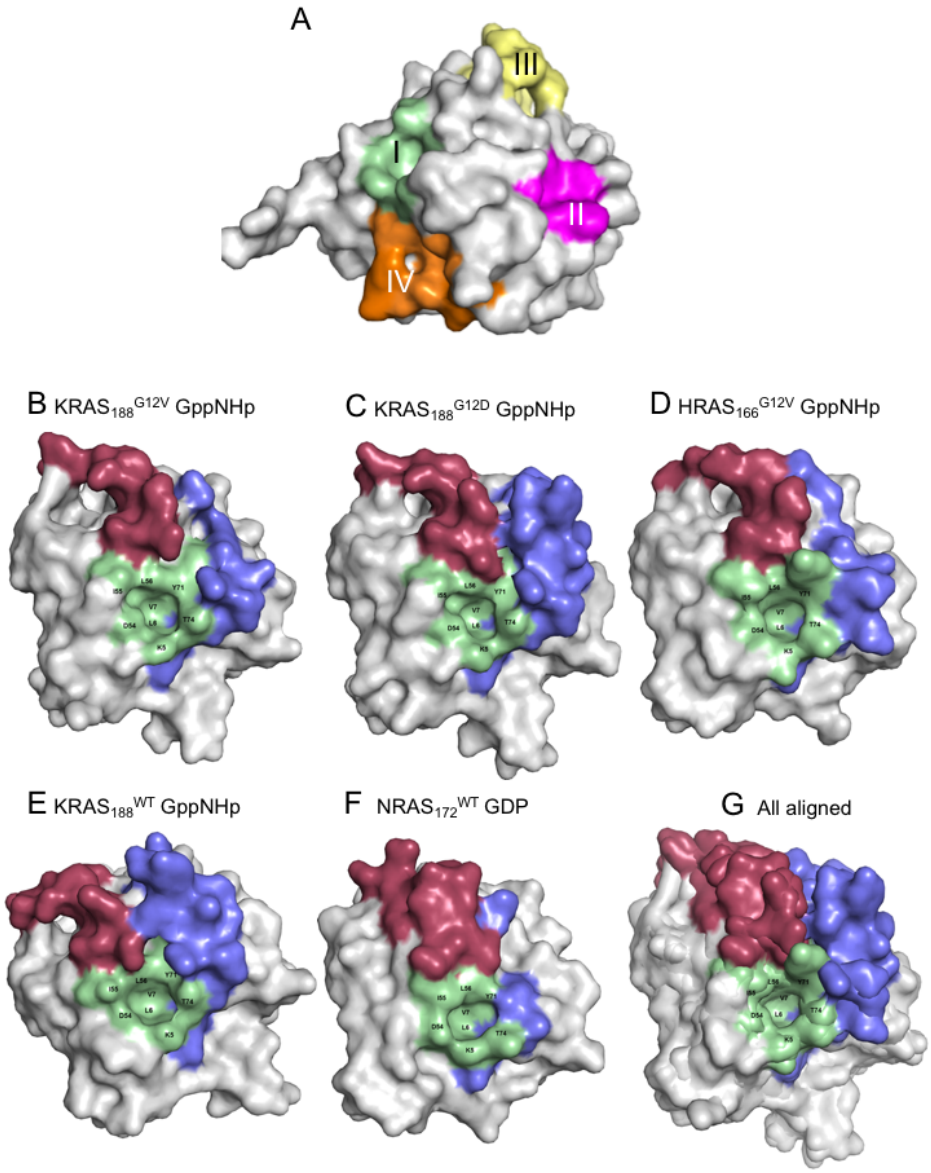

Figure S1. Comparison of potential compound-binding pockets in RAS proteins (wild type and mutant forms)

The structural data for the different RAS proteins and different length proteins has been analyzed to assess potential binding pockets. Four possible pockets exist in full length RAS proteins (Panel A). Pocket I is a hydrophobic pocket near the switch regions; pocket II is a shallow pocket; pocket III is the nucleotide binding pocket and pocket IV is found at the carboxy terminus (evident when full length Ras proteins were analyzed. Pocket I (Sun et al, 2012) is found in K, H and NRAS and different mutant and wild type proteins (Panels B-F) and the topology is very similar in all the proteins as shown by the multi-overlay in Panel G. The panels are B. full length $KRAS_{188}^{G12V}$ (this paper), C. $KRAS_{188}^{G12D}$ (Maurer et al., 2012) and this paper, D. $HRAS_{166}^{G12V}$ (2VH5 $KRAS_{166}^{G12V}$-scFv HRAS) (Tanaka et al., 2007), E. wild type (WT) $KRAS_{188}$ (this paper) and F. full length, wild type $NRAS_{172}$ PDB 3CON. Panel G is a super-imposition of the five structures. Switch I is shown in maroon, switch II in blue and pocket I in green.

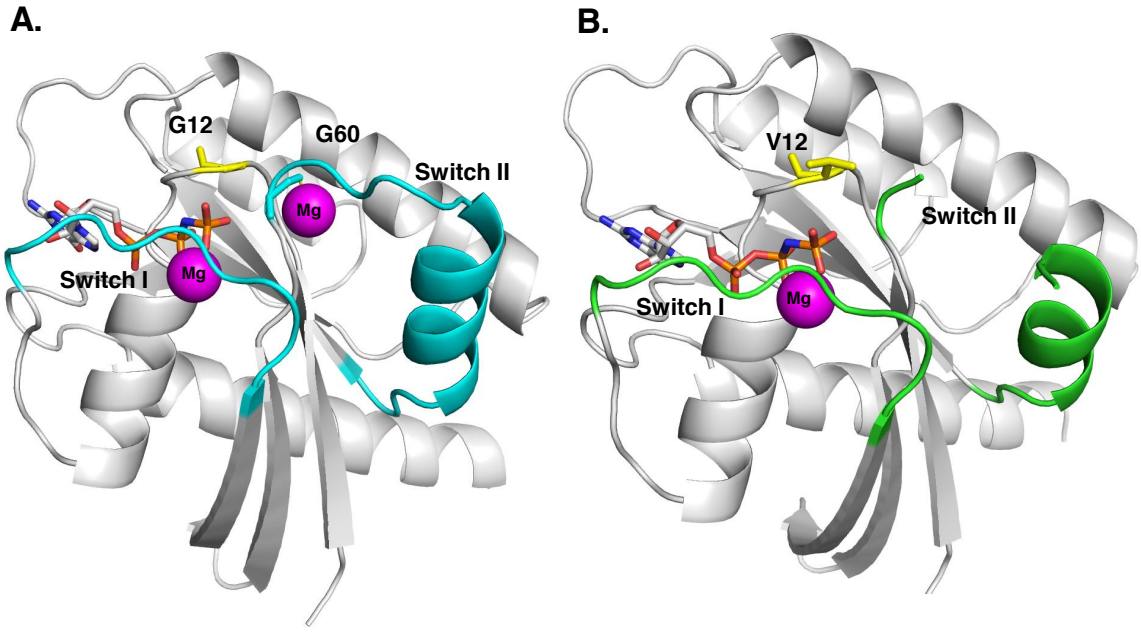

Figure S2. Structure of wild type $KRAS_{188}$ and $KRAS_{188}^{G12V}$ isoforms 4B
Panel A. Ribbon representation of wild type $KRAS_{188}$-GppNHp with the switch regions shown in cyan illustrating the interaction of G60 (depicted in cyan) with the second magnesium ion and stabilizing switch II. Panel B. Ribbon representation of $KRAS_{188}^{G12V}$-GppNHp (switch regions in green). Residues 62 to 66 of switch II are not shown as they are disordered in the maps.

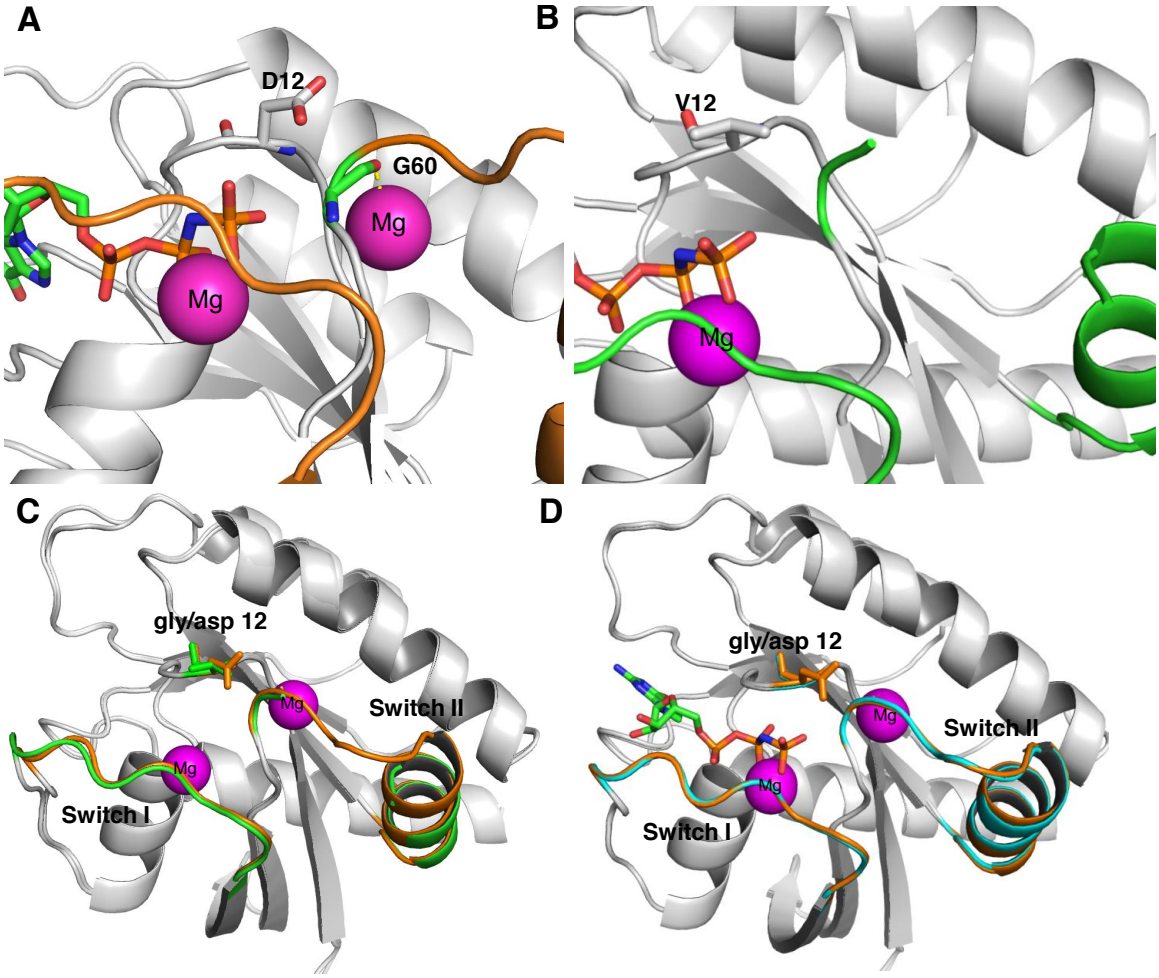

Figure S3. Comparison of the structures of the mutant forms of $KRAS_{188}^{G12D}$ and $KRAS_{188}^{G12V}$

The structures of $KRAS_{188}^{G12D}$ and $KRAS_{188}^{G12V}$ (isoform 4B) are compared in the switch regions with bound GTP-analogue GppNHp.

PANEL A. $KRAS_{188}^{G12D}$ ribbon representation, with Switch I and II in orange, illustrating the interactions of a second Mg ion with G60 found in switch II which stabilize the switch II region. Mg are shown as large magenta spheres.

PANEL B. $KRAS_{188}^{G12V}$ ribbon representation for the switch II region (in green). No second Mg ion was identified in these crystals consistent with an increase in the flexibility of the switch II region of the protein.

PANEL C. Ribbon diagram of an alignment of the $KRAS_{188}^{G12D}$ and G12V. The difference between these structures is the flexibility of the switch II region. $KRAS_{188}^{G12D}$ (switch II shown in orange) has a stable switch II due to the presence of an extra Mg, $KRAS_{188}^{G12V}$ (switch shown in green) has an unstable switch II because of the lack of a second Mg ion around that region.

PANEL D. Ribbon diagram of an alignment of the wild type $KRAS_{188}$ and $KRAS_{188}^{G12D}$. There are no clear differences between these structures, both contain two Mg atoms that gives a higher degree of stability to the switch II regions and the folding is almost identical.

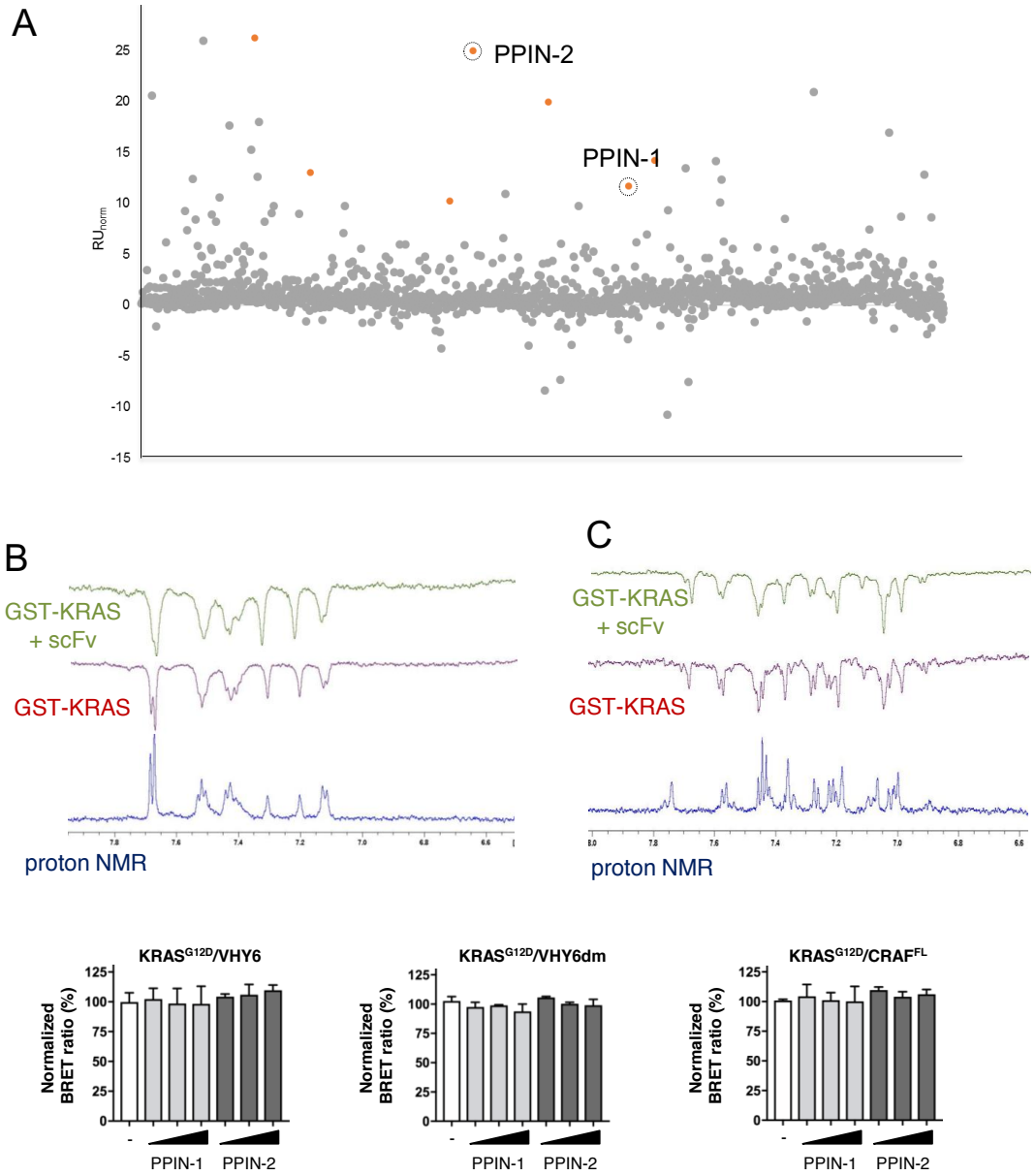

Figure S4. Isolation and characterization of PPIN-1 and -2

The PPI-net compound library (from Prof. Andy Wilson) was screened by SPR at a single concentration and hits PPIN-1 and PPIN-2 identified (panel A, x axis is arbitrary compound position) by binding to $KRAS^{G12V}$-GppNHp) but not to LMO2 proteins. PPIN-1 and 2 were subjected to waterLOGSY analysis (respectively panel B and C) with GST-KRAS (middle, red trace) or GST-KRAS + anti-RAS scFv (top, green trace). The lower trace (blue) is the proton NMR of the compound alone. Panel D show data from BRET assays using RLuc8-$KRAS^{G12D}$ with either anti-RAS VHY6-GFP^2 (left), with de-matured anti-RAS VHY6-GFP^2 (middle) or with GFP^2-$CRAF^{FL}$ (right). The data are computed relative to cells treated with DMSO vehicle only (open boxes) or PPIN-1 (light shaded boxes) and PPIN-2 (dark shaded boxes). The range of concentration of the compounds was 5, 10 and 20μM.

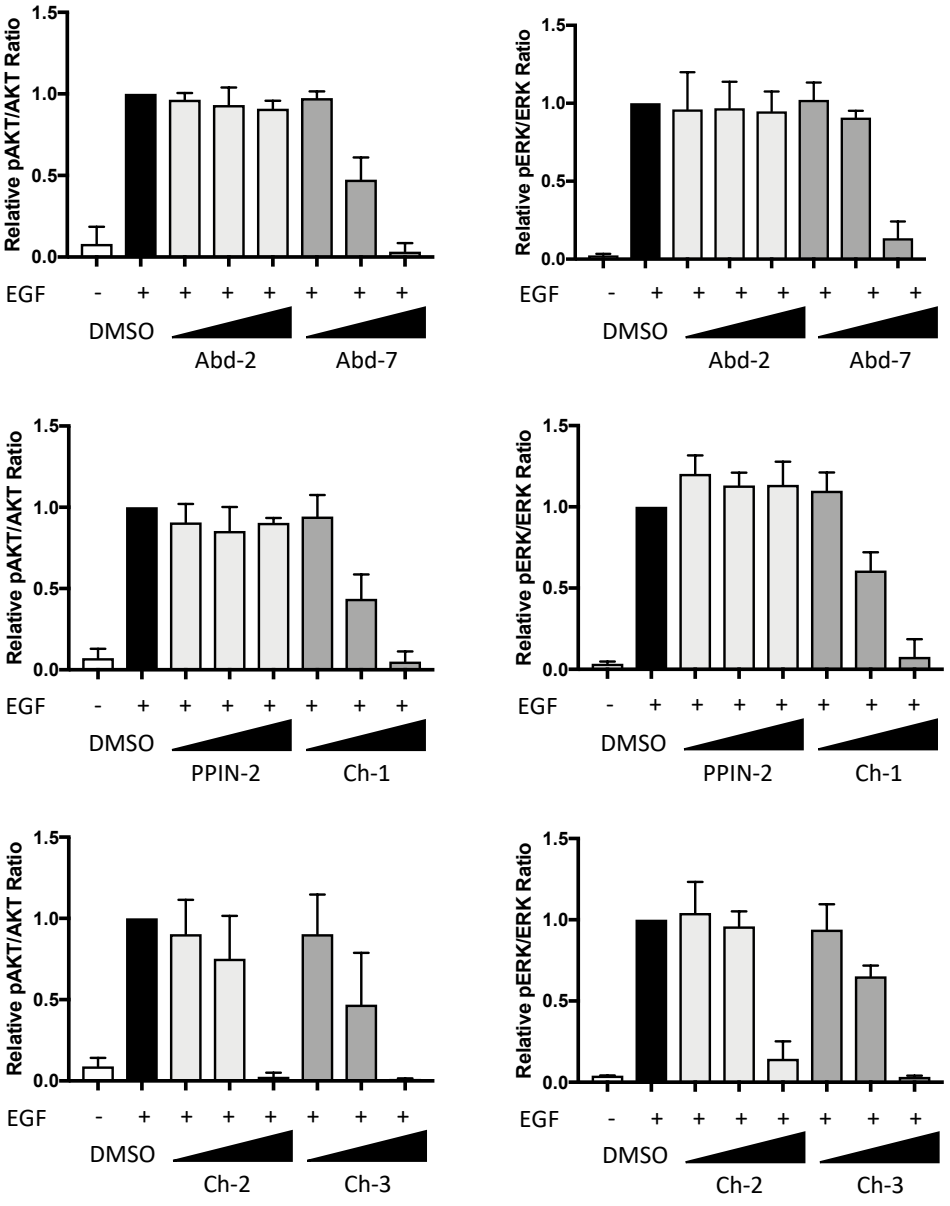

Figure S5: Quantification of data from Western blot data shown in Figure 5

Western blot data were obtained as described in Figure 5. Data were obtained from three independent experiments (biological replicates) and error bars are shown for standard deviations. Images were scanned and quantified using ImageJ software, and the relative quantity of phosphorylated protein was calculated with reference to unphosphorylated protein (eg. pAKT/AKT). The ratios were normalised against the data for DMSO-only control levels.

Compound 1

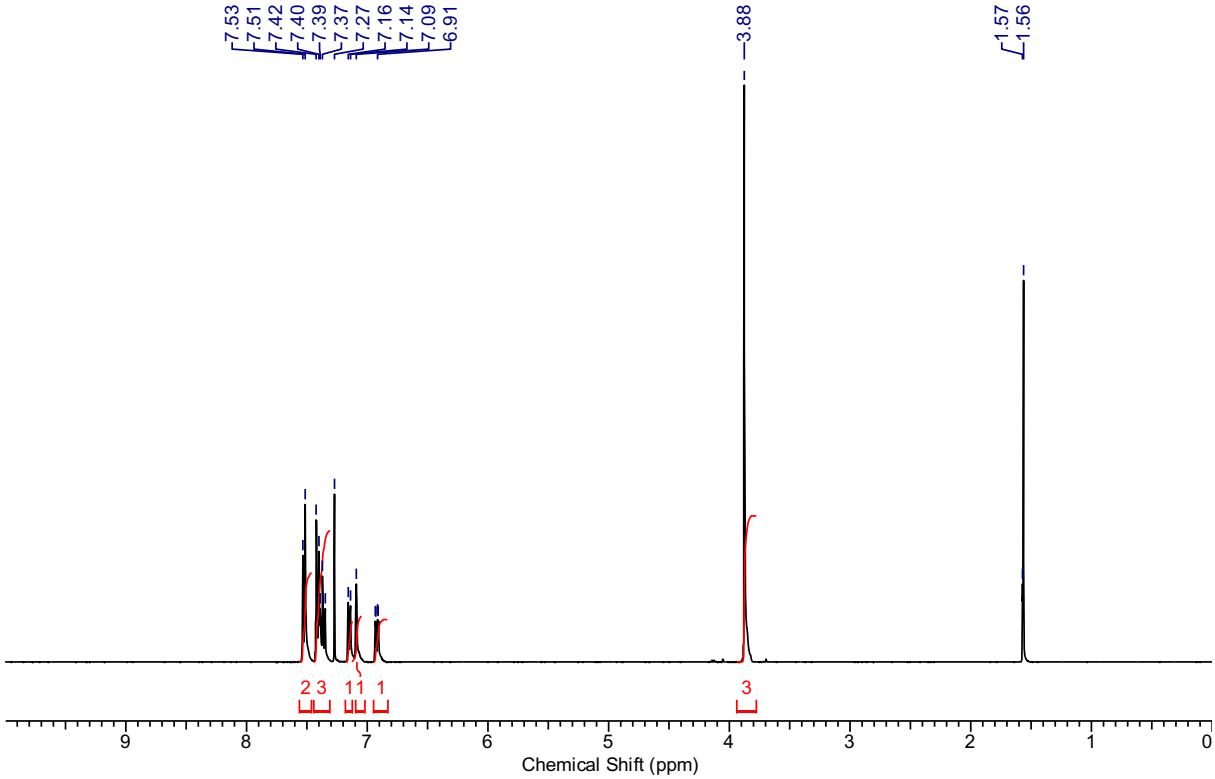
7.53
7.51
7.42
7.40
7.39
7.37
7.27
7.16
7.14
7.09
6.91
3.88
1.57
1.56
2 3 1 1 1
3
9
8
7
6
5
4
3
2
1
0
Chemical Shift (ppm)

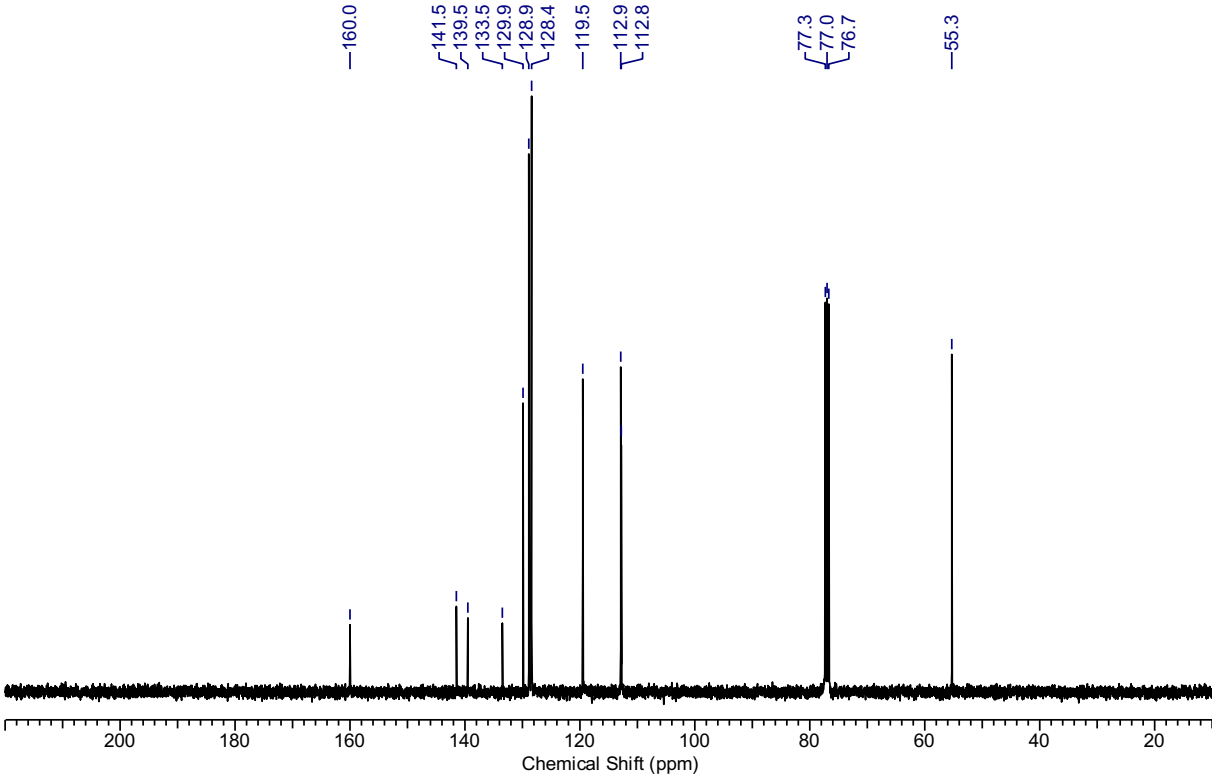
160.0
141.5
139.5
133.5
129.9
128.9
128.4
119.5
112.9
112.8
77.3
77.0
76.7
55.3
200
180
160
140
120
100
80
60
40
20
Chemical Shift (ppm)

Compound Ch-1

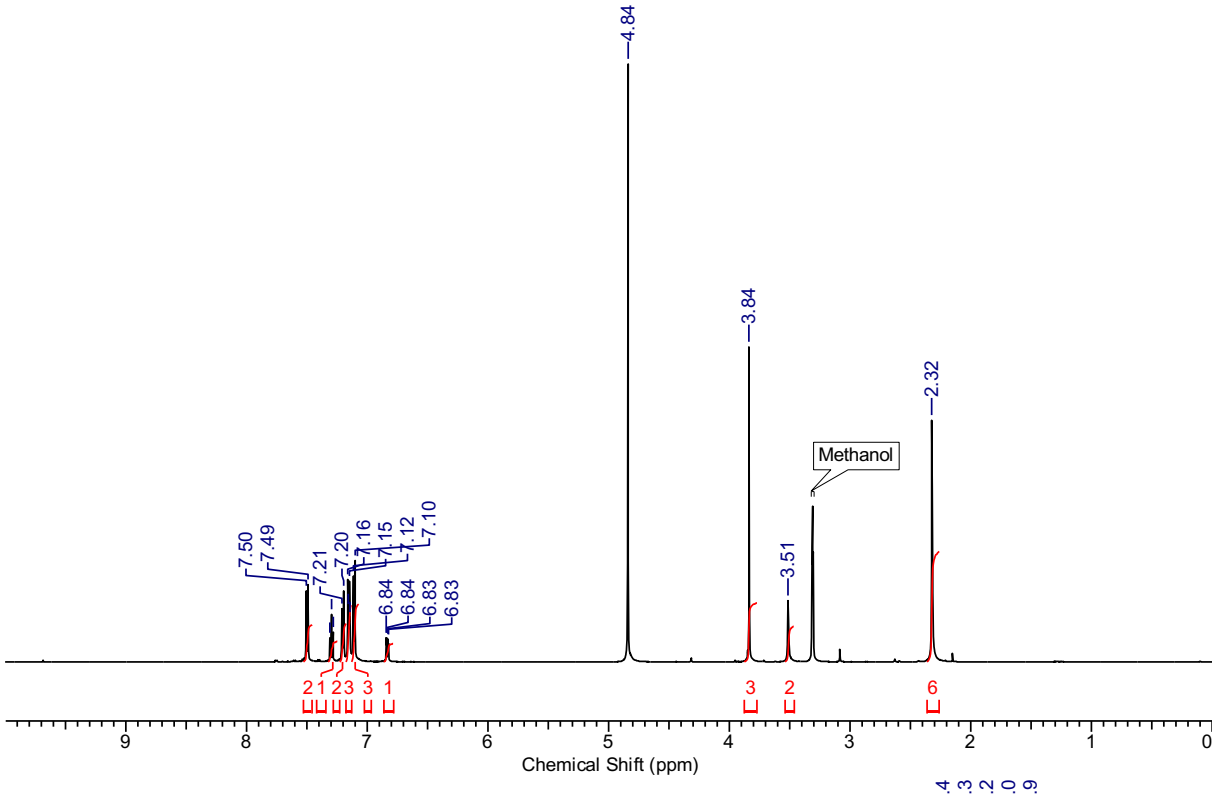

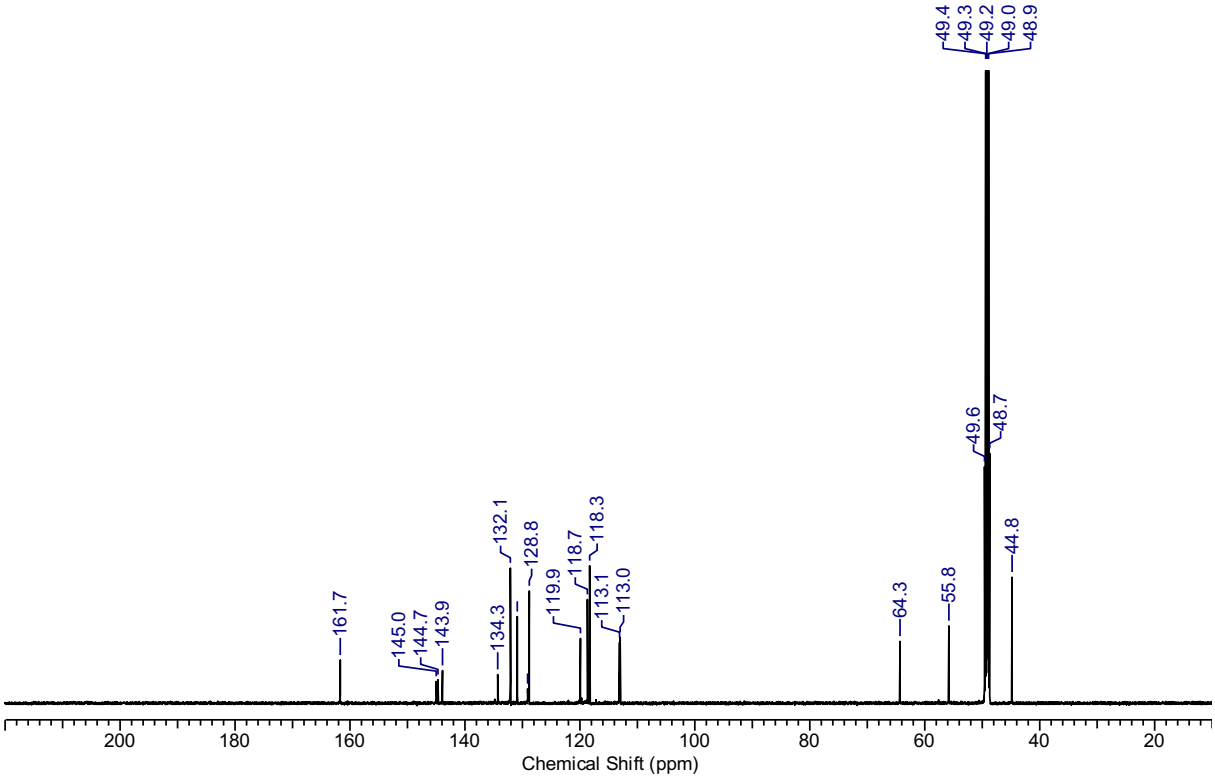

Compound 2

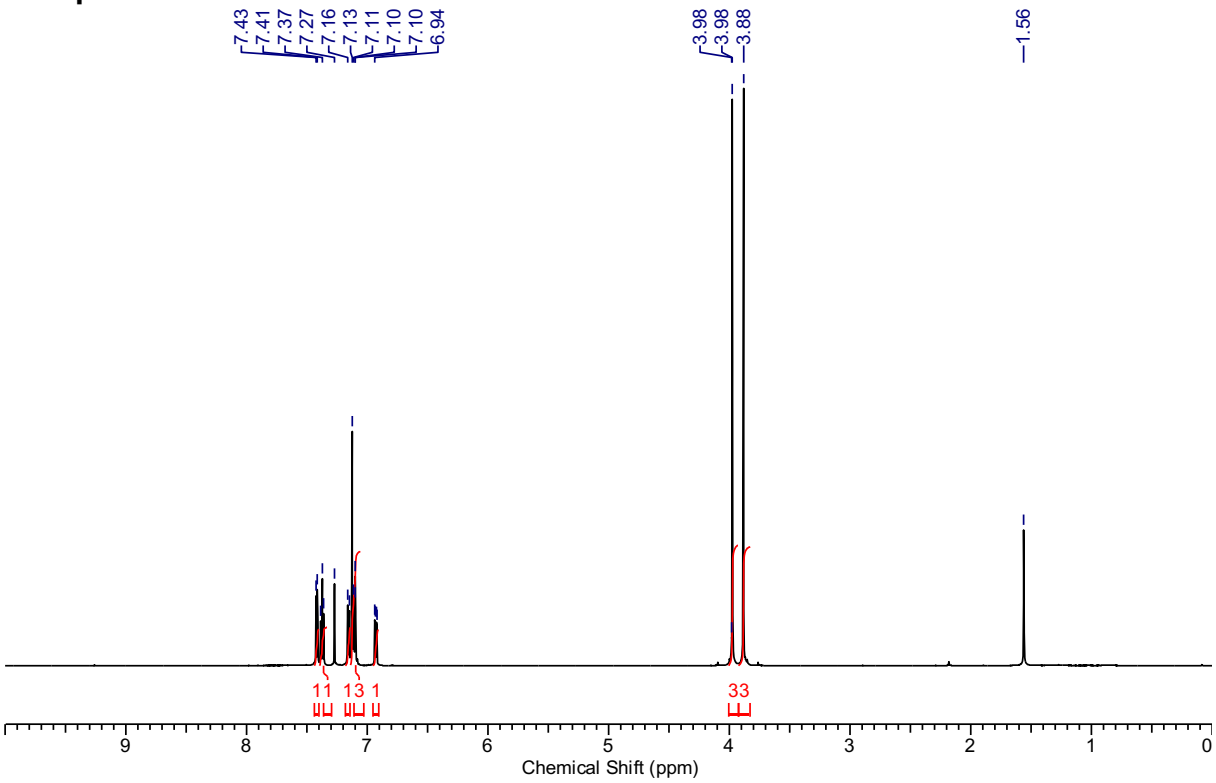
7.43
7.41
7.37
7.27
7.16
7.13
7.11
7.10
7.10
6.94
3.98
3.98
3.88
1.56
11
13
1
33
Chemical Shift (ppm)

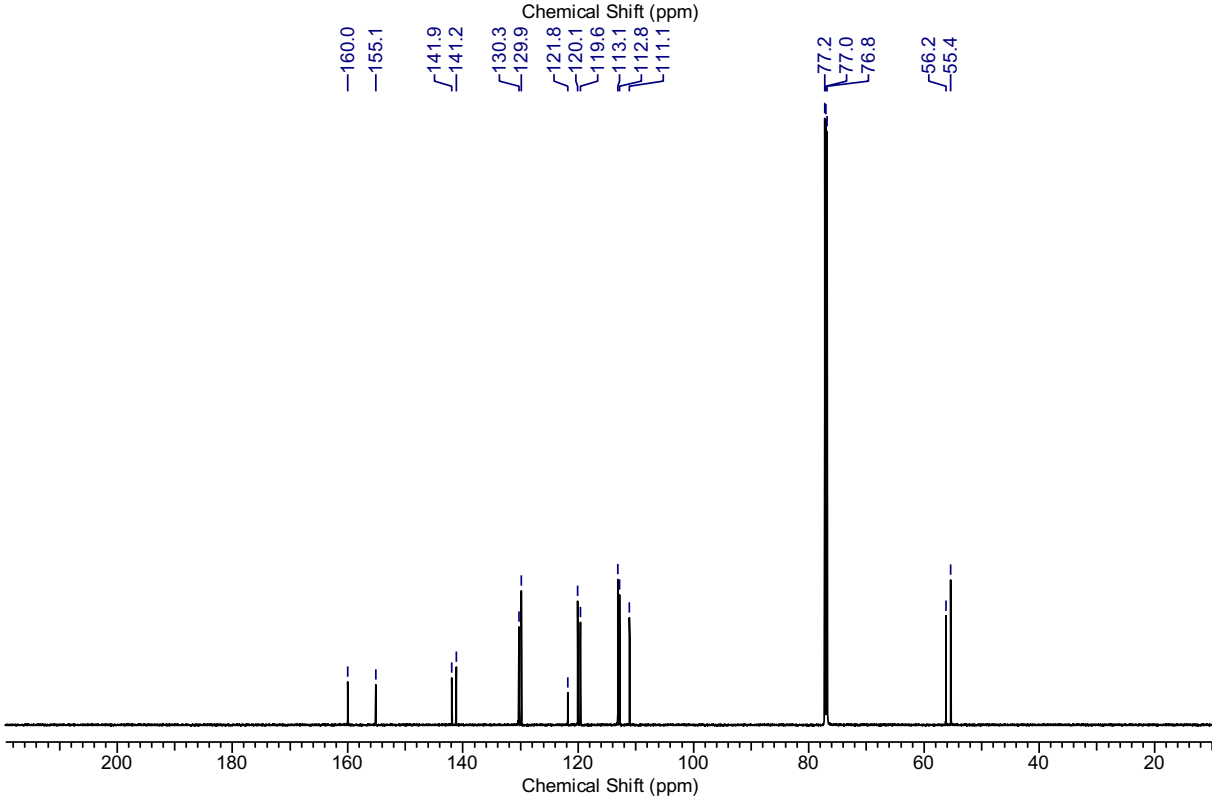
160.0
155.1
141.9
141.2
130.3
129.9
121.8
120.1
119.6
113.1
112.8
111.1
77.2
77.0
76.8
56.2
55.4
Chemical Shift (ppm)

Compound Ch-2

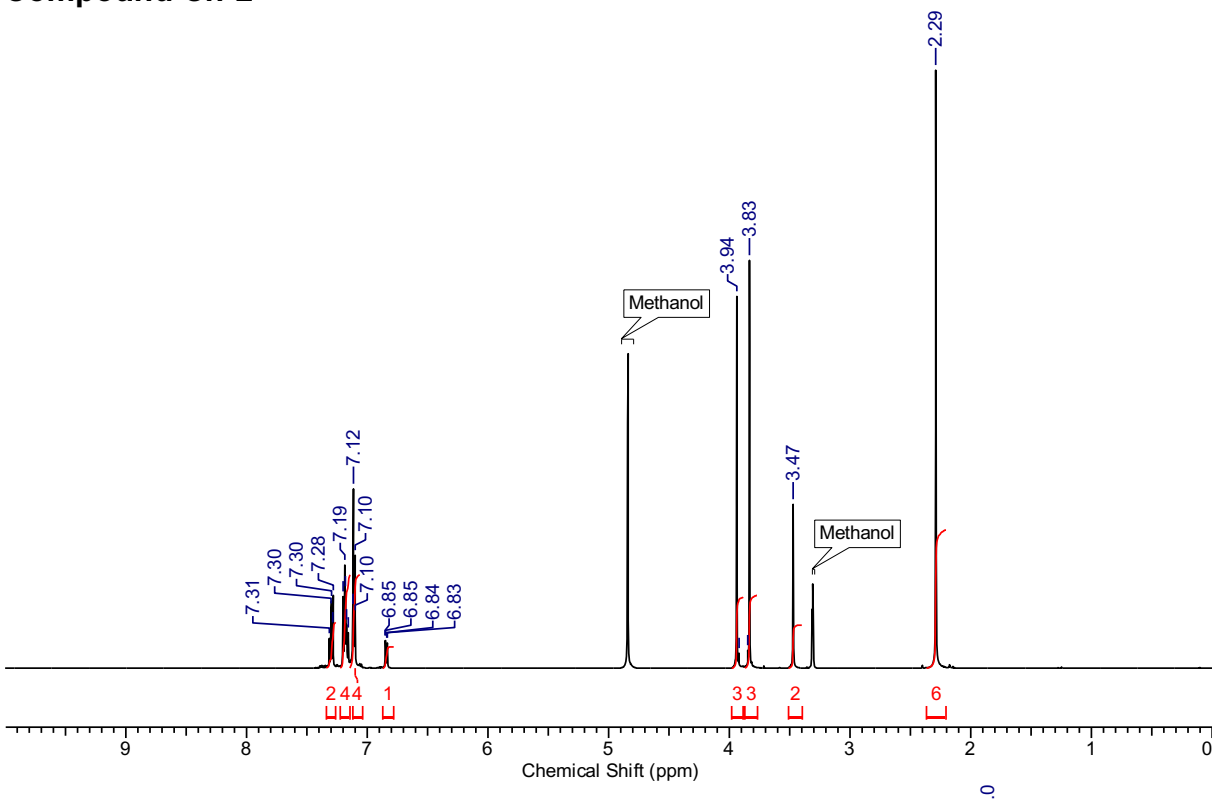

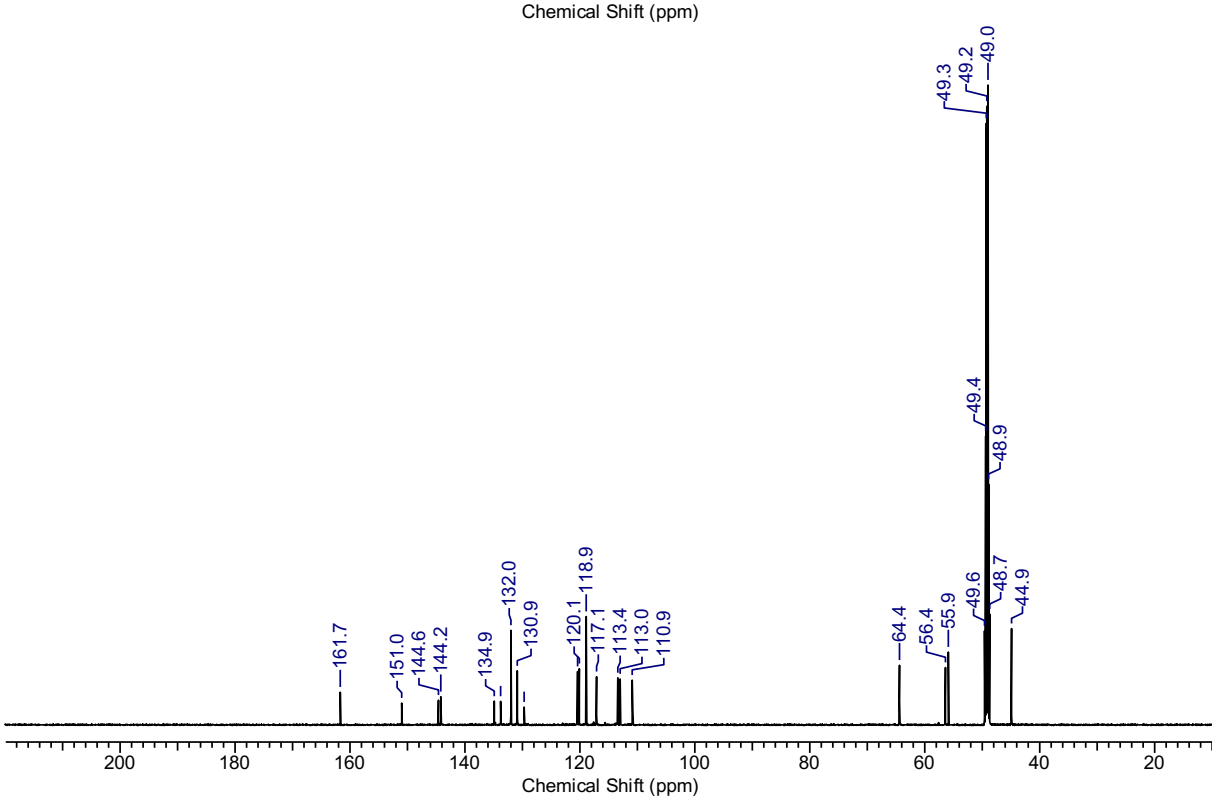

Compound 3

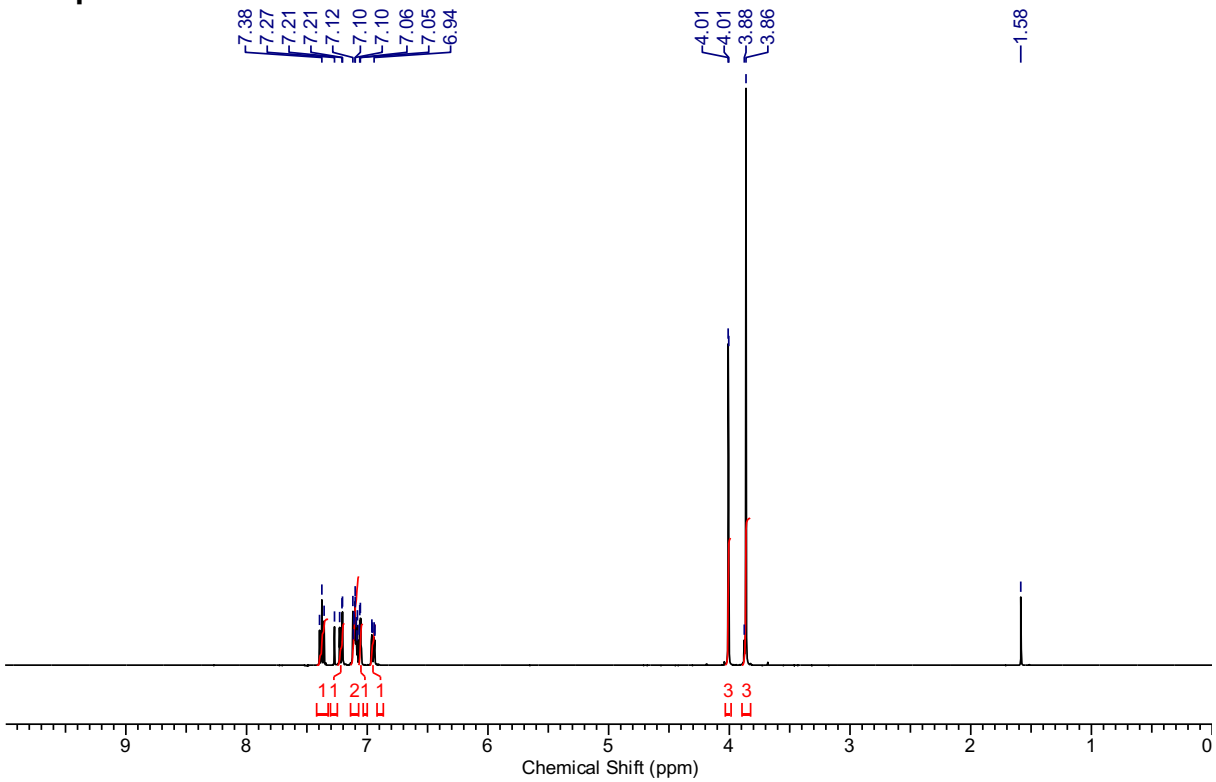
7.38
7.27
7.21
7.21
7.12
7.10
7.10
7.06
7.05
6.94
4.01
4.01
3.88
3.86
1.58
1 1 2 1 1
3 3
Chemical Shift (ppm)

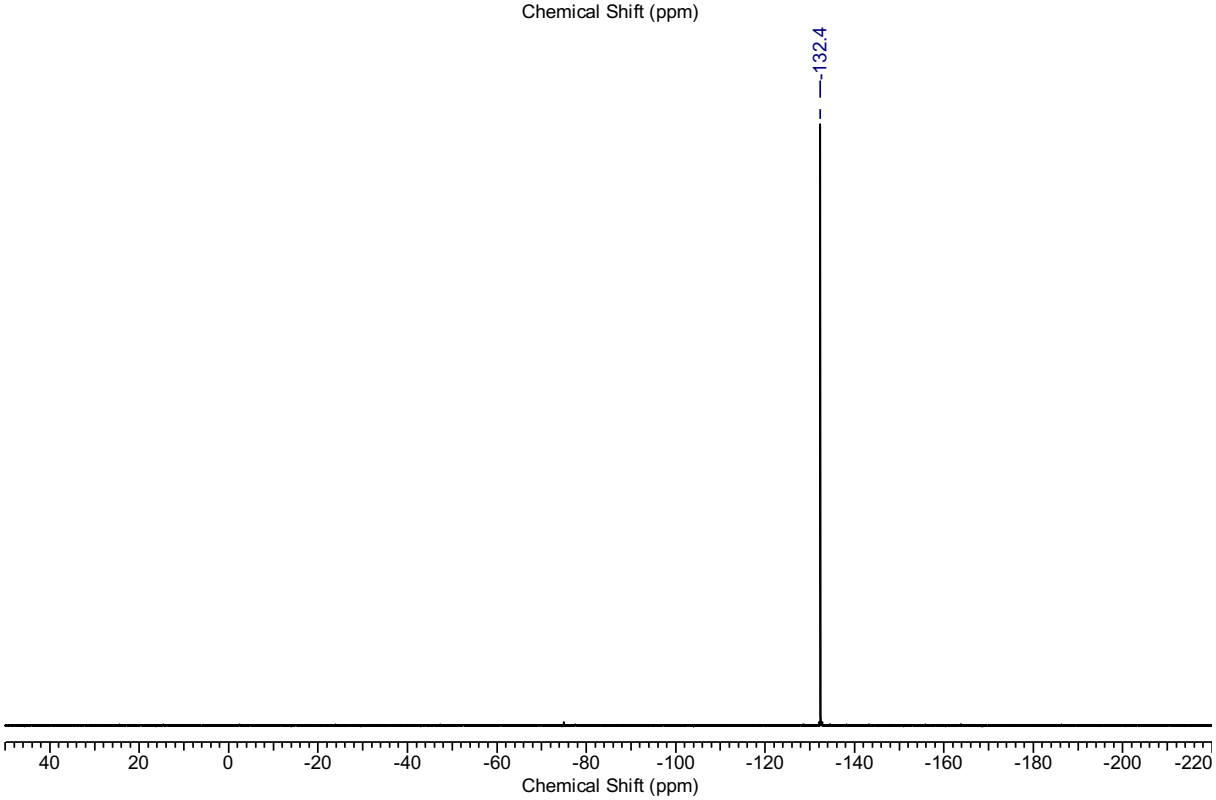
132.4
Chemical Shift (ppm)

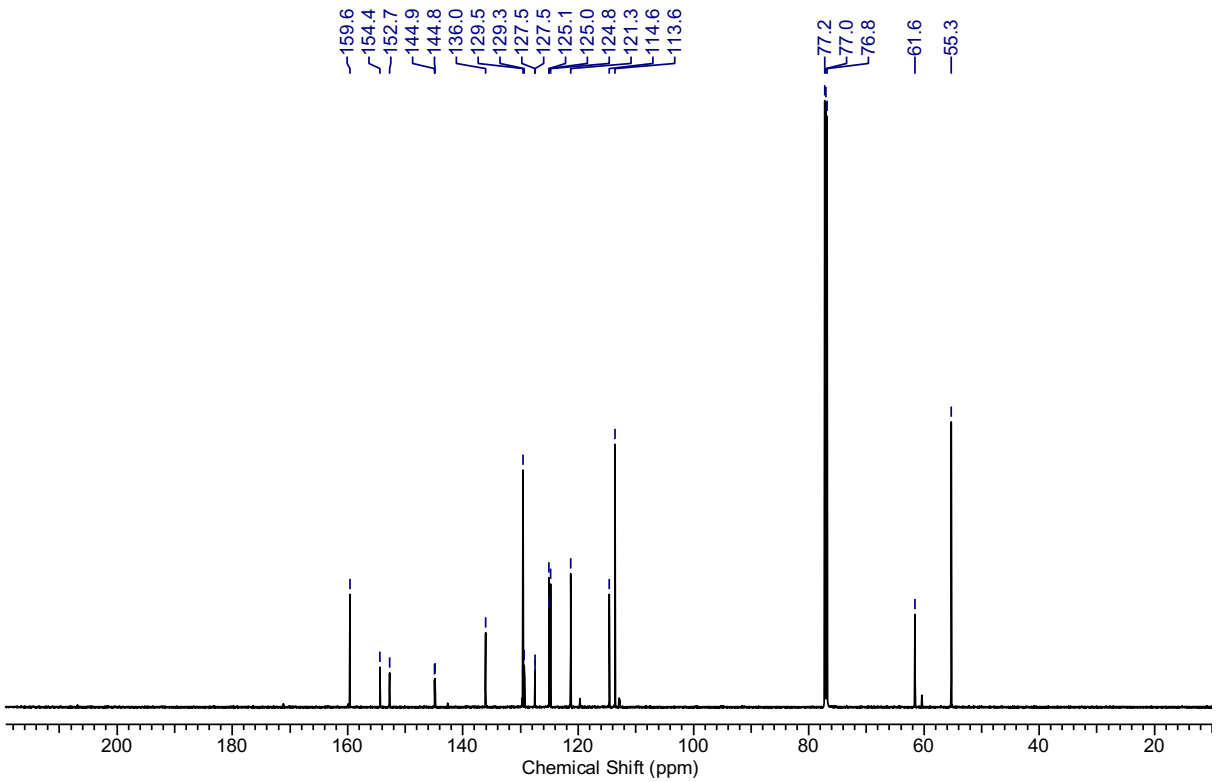
159.6
154.4
152.7
144.9
144.8
136.0
129.5
129.3
127.5
127.5
125.1
125.0
124.8
121.3
114.6
113.6
77.2
77.0
76.8
61.6
55.3
200
180
160
140
120
100
80
60
40
20
Chemical Shift (ppm)

Compound Ch-3

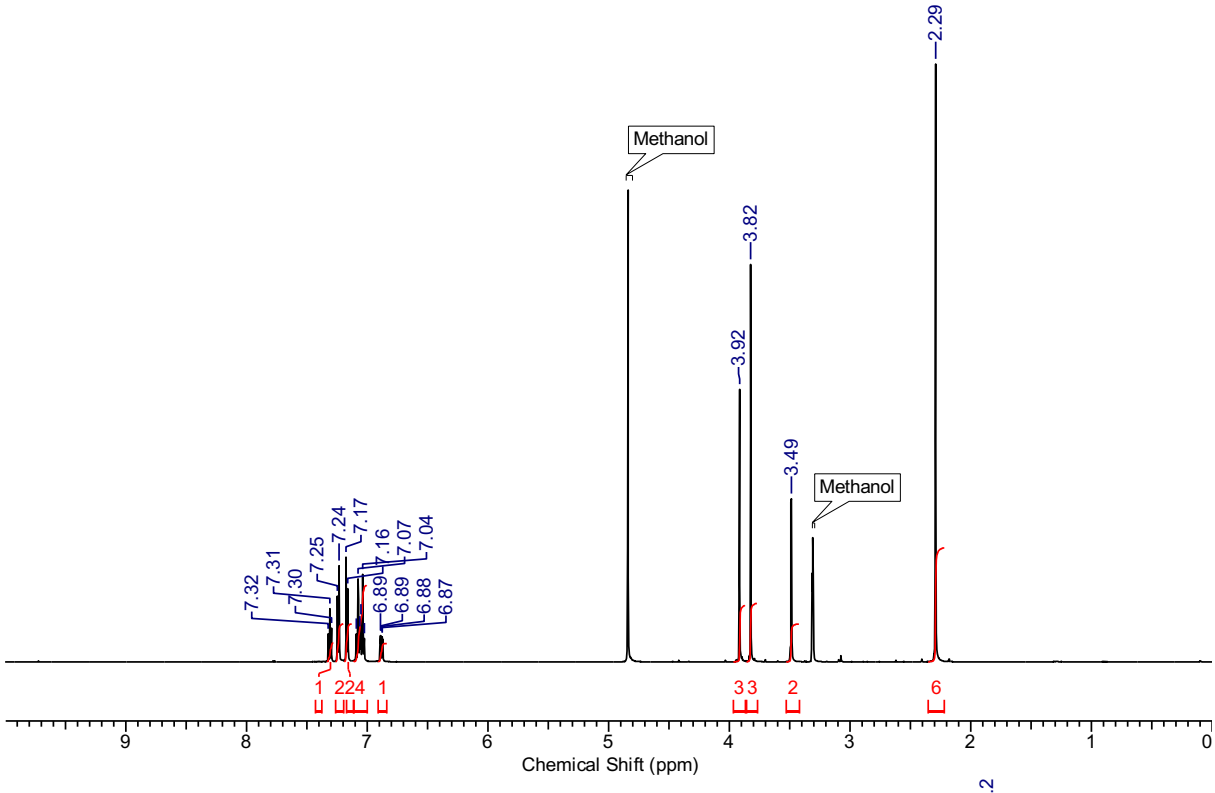

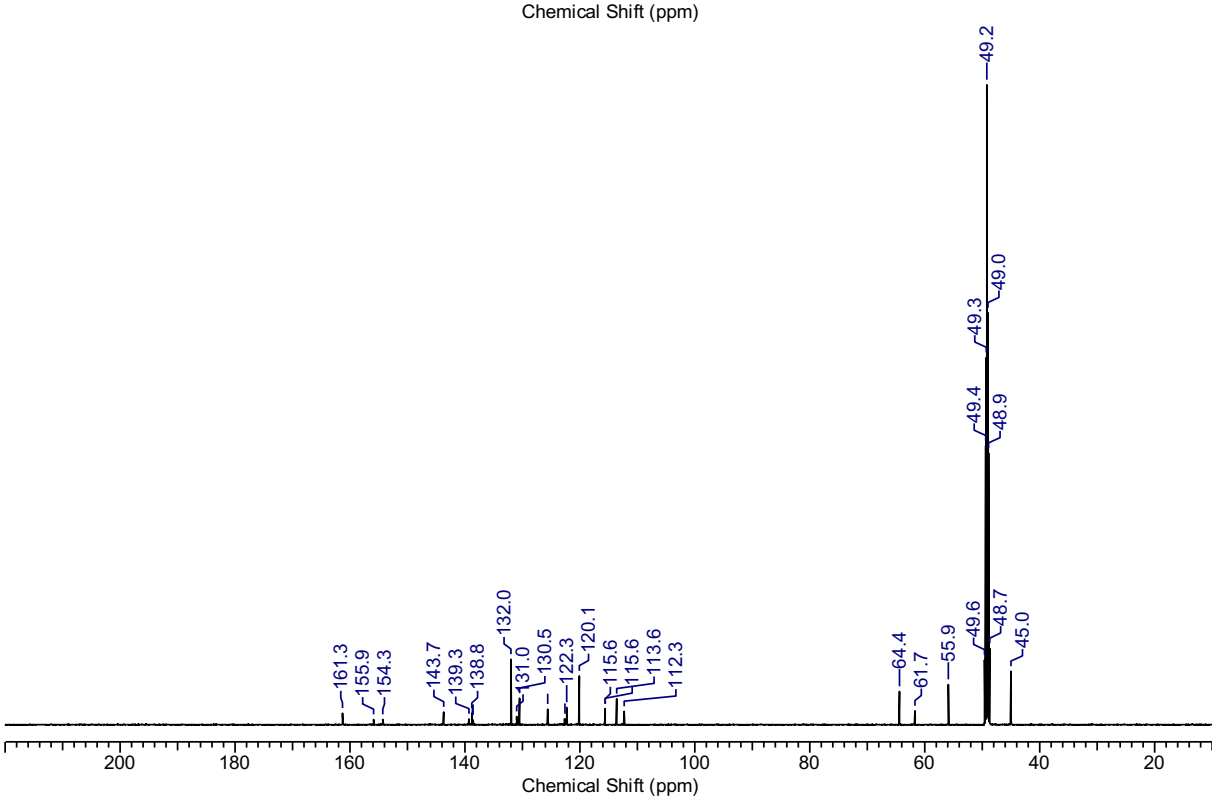

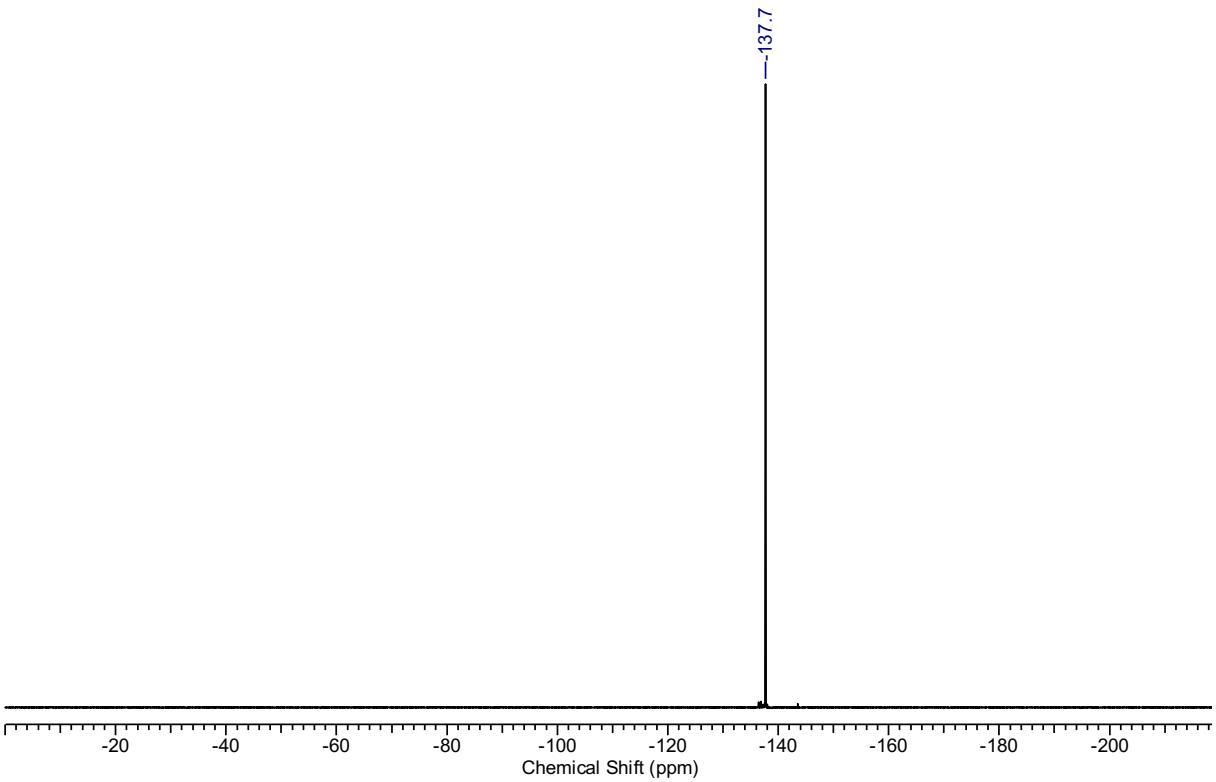

Figure S6. ^{1}H NMR and ^{13}C NMR spectra for all compounds and ^{19}F NMR for compound 3 and Ch-3

NMR spectra were recorded on Bruker Avance spectrometers (AVII400, AVIII400 or AVIIIHD600) in the deuterated solvent stated. The field was locked by external referencing to the relevant deuteron resonance. Chemical shifts (δ) are reported in parts per million (ppm) referenced to the solvent peak.

Table S1. Data processing and refinement statistics for KRAS variant Q61H with bound GTP analogue GPPNHP.

Structure	**$KRAS_{169}^{Q61H}$ GppNHp**
Data Collection	
PDB ID	6GOG
Diffraction source	Beamline i04, DLS
Temperature (K)	100
Wavelength (Å)	0.9795
Space group	P $2_12_12_1$
Molecules/asymmetric unit	6
Unit cell dimensions	
a, b, c (Å)	63.60,118.73,156.57
α, β, γ (°)	90, 90, 90
Resolution range (Å)	94.60 - 2.05 (2.09 - 2.05)
Total No. of reflections	805,732 (24,815)
Unique reflections	74,311 (4,062)
Completeness (%)	98.8 (89.7)
Multiplicity	10.8 (6.1)
Rmeas(I)‡ (%)	18.1 (42.9)
Rmerge‡ (%)	14.9 (33.8)
Rpim(I)§ (%)	7.0 (20.6)
I/sigma	23.7 (4.3)
$CC_{1/2}$	0.994 (0.888)
Refinement	
No. of reflections, working set	70,508 (4,677)
No. of reflections, test set	3,728 (226)
Rwork/Rfree (%)	17.1/19.
No. of atoms	
Protein	8368
Water	715
Average B factors (Å^2)	
Protein	32.26
Ligand	26.32
Solvent	41.66
RMSD	
Bond lengths (Å)	0.012
Bond angles (°)	1.57

Ramachandran plot	
Favoured regions (%)	97.5
Additionally allowed (%)	2.5
Outliers	0.0
MolProbity statistics	
Molprobity score	1.24
Clash score	3.57
Rotamer outliers (%)	0.56

Values in parentheses are for data in the highest resolution shell.

Table S2. Data processing and refinement statistics for full length KRAS structures

Structure	**$KRAS_{188}^{G12V}$ GppNHp**	**$KRAS_{188}^{G12D}$ GppNHp**	**$KRAS_{188}^{WT}$ GppNHp**
Data Collection			
PDB ID	6GOE	6GOF	6GOD
Diffraction source	Beamline i04-1, DLS	Beamline i02, DLS	ID30A-1, ESRF
Temperature (K)	100	100	100
Wavelength (Å)	0.928	0.979	0.966
Space group	H3	H3	H3
Molecules/asymmetric unit	1	1	1
Unit cell dimensions			
a, b, c (Å)	79.88, 79.88, 78.79	78.63, 78.63, 77.54	78.76,78.76,77.18
α, β, γ (°)	90, 90, 120	90, 90, 120	90, 90, 120
Resolution range (Å)	39.94-1.60 (1.64-1.60)	39.31-1.98 (2.03-1.98)	51.11-1.70(1.73-1.70)
Total No. of reflections	126628(9332)	126182 (8935)	57807(3104)
Unique reflections	24651(1820)	12435 (900)	18963 (965)
Completeness (%)	99.7 (99.8)	99.9 (100.0)	98.0 (99.6)
Multiplicity	5.1 (5.1)	10.1 (9.9)	3.0 (3.2)
Rmeas(I)‡ (%)	0.098(1.196)	0.171 (1.480)	0.062(0.566)
Rmerge‡ (%)	0.088(1.072)	0.152 (1.324)	0.051 (0.468)
Rpim(I)§ (%)	0.043 (0.526)	0.054 (0.468)	0.034 (0.311)
I/sigma	9.4(1.5)	11.2 (1.7)	11.1 (2.3)
$CC_{1/2}$	0.996 (0.528)	0.997 (0.555)	0.998(0.704)
Refinement			
No. of reflections, working set	24651 (2450)	12434 (1225)	18914 (1899)
No. of reflections, test set	1188 (112)	584 (72)	988 (115)
Rwork/Rfree (%)	0.183/0.220	0.181/ 0.249	0.181/ 0.236
No. of atoms			
Protein	1332	1382	1384
Water	112	117	101
Average B factors (Å^2)			
Protein	31.27	38.54	34.07
Ligand	21.44	26.90	26.91

Solvent	38.14	39.86	42.11
RMSD			
Bond lengths (Å)	0.023	0.013	0.020
Bond angles (°)	2.09	1.56	2.02
Ramachandran plot			
Favoured regions (%)	98.2	98.2	97.1
Additionally allowed (%)	1.8	1.8	2.9
Outliers	0.00	0.00	0.00
MolProbity statistics			
Molprobity score	1.09	1.08	1.51
Clash score	0.37	2.15	2.49
Rotamer outliers (%)	4.03	1.30	2.60

Values in parentheses are for data in the highest resolution shell.

Table S3. Data processing and refinement statistics for binding of compounds PPIN-1 and PPIN-2 to $KRAS_{169}^{Q61H}$

Structure	**$KRAS_{169}^{Q61H}$ + PPIN-1**	**$KRAS_{169}^{Q61H}$ + PPIN2**
Data Collection		
PDB ID	6GOM	6GQT
Diffraction source	Beamline i04-1, DLS	Beamline i04-1, DLS
Wavelength (Å)	0.9282	0.9282
Space group	$P2_12_12_1$	$P2_12_12_1$
Molecules/asymmetric unit	6	6
Unit cell dimensions		
a, b, c (Å)	64.18, 119.84, 158.60	64.27, 119.55, 158.59
α, β, γ (°)	90, 90, 90	90, 90, 90
Resolution range (Å)	66.13-1.63 (1.67-1.63)	59.8-1.69 (1.73-1.69)
Total No. of reflections	1,896,813 (67,739)	1,746,677 (70,866)
Unique reflections	152,914 (7,534)	137,251 (6764)
Completeness (%)	100 (99.3)	100 (100)
Multiplicity	12.4 (9.0)	12.7 (10.5)
Rmeas(I) ǂ (%)	8.8 (186)	11 (215)
Rmerge‡ (%)	8.8 (176)	10.6 (204)
Rpim(I) § (%)	2.5 (61.6)	3.1 (66.4)
I/sigma	15.9 (1.1)	15.3 (1.2)
$CC_{1/2}$	1 (0.5)	1 (0.6)
Refinement		
No.of reflections, working set	145,381	130,344
No. of reflections, test set	7428	6817
Rwork/Rfree (%)	18.6/20.7	18.8/21.1
No. of atoms		
Protein	8100	8144
Water	776	814
Average B factors (Å2)		
Protein	34.9	36.127
Ligand	38.2	98.2
Water	42.2	43.2
RMSD		
Bond lengths (Å)	0.02	0.02
Bond angles (°)	1.98	1.91
Ramachandran plot		

Favoured regions (%)	97.9	97.6
Additionally allowed (%)	2.1	2.4
Outliers	0	0
MolProbity statistics		
Molprobity score	0.94	1.22
Clash score	1.75	2.56
Rotamer outliers (%)	0.94	1.4

Values in parentheses are for data in the highest resolution shell.

Table S4. Data processing and refinement statistics for binding of compounds Ch-1, Ch-2 and Ch-3 to $KRAS^{Q61H}$

Structure	$KRAS_{169}^{Q61H}$ + Ch-1	$KRAS_{169}^{Q61H}$ + Ch-2	$KRAS_{169}^{Q61H}$ + Ch-3
Data Collection			
PDB ID	6GQW	6GQX	6GQY
Diffraction source	Beamline P14, DESY	Beamline P14, DESY	Beamline P14, DESY
Wavelength (Å)	0.9763	0.9763	0.9763
Space group	$P2_12_12_1$	$P2_12_12_1$	$P2_12_12_1$
Molecules/asymmetric unit	6	6	6
Unit cell dimensions			
a, b, c (Å)	63.48, 118.54, 156.53	63.19, 118.03, 156.37	63.53, 118.68, 157.00
α, β, γ (°)	90, 90, 90	90, 90, 90	90, 90, 90
Resolution range (Å)	94.5-2.8 (2.95-2.8)	156-2.2 (2.26-2.20)	118-2.75 (2.88-2.75)
Total No. of reflections	202,993 (29,729)	577,336 (38,536)	332,585 (45,297)
Unique reflections	27,994 (4,121)	60,229 (4,369)	31,557 (4,134)
Completeness (%)	92.9 (95.8)	100 (99.8)	99.8 (99.9)
Multiplicity	7.3 (7.2)	9.6 (8.8)	10.5 (11.0)
Rmeas(I)‡ (%)	16.9 (96.1)	10.8 (93.9)	15.9 (59.1)
Rmerge‡ (%)	14.6 (83.3)	9.7 (83.0)	14.3 (53.5)
Rpim(I)§ (%)	8.4(47.5)	4.7 (43.2)	6.7 (24.5)
I/sigma	12.3 (3.7)	15.6 (3.3)	16.0 (4.2)
$CC_{1/2}$	0.99 (0.83)	0.998 (0.908)	0.997 (0.916)
Refinement			
No.of reflections, working set	26,537	57,101	29,946
No. of reflections, test set	1,403	3,016	1,561
Rwork/Rfree (%)	18.9/22.4	20.3/23.0	20.5/24.7
No. of atoms			
Protein	8319	8202	8289
Water	36	95	33
Average B factors			
Protein	54.6	43.6	46.3
Ligand	33.6	47.5	60.0
Water	78.5	31.7	33.5
RMSD			
Bond lengths (Å)	0.01	0.01	0.01
Bond angles (°)	1.36	1.45	1.5
Ramachandran plot			

Favoured regions (%)	97.3	97.5	96.6
Additionally allowed (%)	2.7	2.5	3.4
Outliers	0	0	0
MolProbity statistics			
Molprobity score	1.37	1.24	1.42
Clash score	2.77	2.95	2.34
Rotamer outliers (%)	1.7	1.2	1.7

Values in parentheses are for data in the highest resolution shell.

Table S5. Compound properties for comparison

	Abd-7	**PPN-1**	**PPN-2**	**Ch-1**	**Ch-2**	**Ch-3**
L.E.	0.34	0.30	0.27	N/A	0.35	N/A
Cell Viability (μM, 48 h)	10.8	Inactive	Inactive	9.5	9.9	7.8
Cell Viability (μM, 72 h)	8.2	Inactive	Inactive	5.3	7.2	4.5

References

1. Hermann C, Horn G, Spaargaren M, & Wittinghofer A (1996) Differential interaction of the ras family GTP-binding proteins H-RAs, Rap1A, and R-Ras with the putative effector molecules Raf kinase and Ral-guanine nucleotide exchange factor. *J Biol Chem* 271:6794-6800.
2. Luft JR & DeTitta GT (1999) A method to produce microseed stock for use in the crystallization of biological macromolecules. *Acta Crystallogr D Biol Crystallogr* 55(Pt 5):988-993.
3. McCoy AJ*, et al.* (2007) Phaser crystallographic software. *J Appl Crystallogr* 40(Pt 4):658-674.
4. Murshudov GN, Vagin AA, & Dodson EJ (1997) Refinement of macromolecular structures by the maximum-likelihood method. *Acta Crystallogr D Biol Crystallogr* 53(Pt 3):240-255.
5. Emsley P, Lohkamp B, Scott WG, & Cowtan K (2010) Features and development of Coot. *Acta Crystallogr D Biol Crystallogr* 66(Pt 4):486-501.
6. Chen VB*, et al.* (2010) MolProbity: all-atom structure validation for macromolecular crystallography. *Acta Crystallogr D Biol Crystallogr* 66(Pt 1):12-21.
7. Laskowski RA, MacArthur MW, Moss DS, & Thornton JM (1993) PROCHECK - a program to check the stereochemical quality of protein stuctures. *J. App. Cryst.* 26(283-291).
8. Adams PD*, et al.* (2010) PHENIX: a comprehensive Python-based system for macromolecular structure solution. *Acta Crystallogr D Biol Crystallogr* 66(Pt 2):213-221.
9. Dalvit C, Fogliatto G, Stewart A, Veronesi M, & Stockman B (2001) WaterLOGSY as a method for primary NMR screening: practical aspects and range of applicability. *J Biomol NMR* 21(4):349-359.
10. Cheeseright T, Mackey M, Rose S, & Vinter A (2006) Molecular Field Extrema as Descriptors of Biological Activity: Definition and Validation. *J. Chem. Inf. Model.* 46:665-676.
11. Bery N*, et al.* (2018) BRET-based RAS biosensors that show a novel small molecule is an inhibitor of RAS-effector protein-protein interactions. *Elife* 7. doi.org/10.7554/eLife.37122